



HAL
open science

Atmospheric Deposition Over the Caribbean Region: Sea Salt and Saharan Dust Are Sources of Essential Elements on the Island of Guadeloupe

Yangjunjie Xu-Yang, Céline Dessert, Rémi Losno

► **To cite this version:**

Yangjunjie Xu-Yang, Céline Dessert, Rémi Losno. Atmospheric Deposition Over the Caribbean Region: Sea Salt and Saharan Dust Are Sources of Essential Elements on the Island of Guadeloupe. *Journal of Geophysical Research: Atmospheres*, 2022, 127 (22), 10.1029/2022JD037175 . hal-03944911

HAL Id: hal-03944911

<https://cnrs.hal.science/hal-03944911>

Submitted on 16 Mar 2023

HAL is a multi-disciplinary open access archive for the deposit and dissemination of scientific research documents, whether they are published or not. The documents may come from teaching and research institutions in France or abroad, or from public or private research centers.

L'archive ouverte pluridisciplinaire **HAL**, est destinée au dépôt et à la diffusion de documents scientifiques de niveau recherche, publiés ou non, émanant des établissements d'enseignement et de recherche français ou étrangers, des laboratoires publics ou privés.



Distributed under a Creative Commons Attribution 4.0 International License

Atmospheric Deposition Over the Caribbean Region: Sea Salt and Saharan Dust Are Sources of Essential Elements on the Island of Guadeloupe

Yangjunjie Xu-Yang¹ , Céline Dessert¹, and Rémi Losno¹ 

¹Université Paris Cité, Institut de physique du globe de Paris, CNRS, Paris, France

Key Points:

- We have monitored atmospheric deposition in Guadeloupe over a 3-year period with measurements of Al, Na, Mg, P, S, K, Ca, Fe, and Zn
- Strong seasonality for Saharan dust, no inter-annual deposition flux variations for both sea salt and Saharan dust
- We suggest that the contributions of Saharan dust, sea salt, and biogenic emissions explain the origin of the deposited elements

Supporting Information:

Supporting Information may be found in the online version of this article.

Correspondence to:

Y. Xu-Yang,
xuyangjunjie@gmail.com

Citation:

Xu-Yang, Y., Dessert, C., & Losno, R. (2022). Atmospheric deposition over the Caribbean region: Sea salt and Saharan dust are sources of essential elements on the island of Guadeloupe. *Journal of Geophysical Research: Atmospheres*, 127, e2022JD037175. <https://doi.org/10.1029/2022JD037175>

Received 23 MAY 2022

Accepted 28 OCT 2022

Author Contributions:

Conceptualization: Céline Dessert, Rémi Losno

Data curation: Céline Dessert, Rémi Losno

Formal analysis: Céline Dessert, Rémi Losno

Funding acquisition: Céline Dessert

Investigation: Céline Dessert, Rémi Losno

Methodology: Céline Dessert, Rémi Losno

Project Administration: Céline Dessert

Resources: Céline Dessert, Rémi Losno

Validation: Céline Dessert, Rémi Losno

© 2022. The Authors.

This is an open access article under the terms of the [Creative Commons Attribution License](https://creativecommons.org/licenses/by/4.0/), which permits use, distribution and reproduction in any medium, provided the original work is properly cited.

Abstract Dust emitted from North Africa is transported over long distances and has a strong impact on large areas over the North Tropical Atlantic Ocean. Sea salt emitted by the sea surface is the second source of essential elements transported in the atmosphere and plays a major role in the cycles of alkaline-earth metals in the ecosystems of tropical North Atlantic Islands. The total atmospheric deposition fluxes were continuously sampled on a weekly basis in Guadeloupe, Lesser Antilles, from March 2015 to August 2018 (41 months). Elemental deposition fluxes, including Al, Ca, K, Mg, Fe, Na, P, S, and Zn, were measured for all samples to provide the first long time series of atmospheric elemental deposition fluxes over the Lesser Antilles region. It is shown that: (a) the three sources of atmospheric deposits in Guadeloupe for the presented elements are sea salt (for K, Ca, Mg, Na, and S), long-range transported Saharan dust (for Al, Ca, K, and Fe), and biogenic particles (for P and Zn); (b) the average deposition mass fluxes of sea salt and Saharan dust are 17.4 and 11.2 g.m⁻².year⁻¹, respectively, without noticeable inter-annual variations; (c) a pronounced seasonality is found for the Saharan dust deposition, for which maximum flux values are observed between June and July each year and 85% of the annual deposition flux occurs between April and September; (d) the deposition flux of sea salt is strongly correlated to local wind speed, without seasonality.

Plain Language Summary Saharan dust and sea salt contribute toward feeding trees living on Caribbean Island ground with alkaline, alkaline-earth cations and other important elements. Saharan dust is transported time to time from North Africa with a higher frequency of events in summer. Sea salt is continuously locally emitted from the sea surface by the action of trade winds and storms on the sea surface that produces sea water brine. For the first time, we have measured the Saharan dust and sea salt deposition flux continuously for 3 years in Guadeloupe. We have found that Saharan dust brings iron, calcium, and potassium, and sea salt brings sodium, magnesium, sulfur, and potassium. The high flux of phosphorus is due to the local recycling of living debris and zinc which probably come from sea surface micro-layer torn by the wind. These results enhance our knowledge of nutrients cycles in the North Atlantic region.

1. Introduction

Atmospheric deposition is a source of nutrients and metals for terrestrial plant development (e.g., Alvarado, 2015; Hedin et al., 1994; Kennedy et al., 1998; Okin et al., 2004) as well as phytoplankton growth in the open ocean (e.g., Martin & Fitzwater, 1988; Okin et al., 2011). Studies conducted in tropical areas have suggested that atmospheric deposits are major sources of nutrients such as phosphorus, potassium, calcium, magnesium, iron, and sulfur in ecosystems: this significant input has been particularly observed for the island of Hawaii (Chadwick et al., 1999; Kennedy et al., 1998), the Amazon Basin (Abouchami et al., 2013; Barkley et al., 2019; Koren et al., 2006; Prospero et al., 2020; Yu, Chin, Yuan, et al., 2015) and the Caribbean Basin (Dessert et al., 2015, 2020; Kandler et al., 2018; Kumar et al., 2014; McClintock et al., 2015, 2019; Pett-Ridge, Derry, & Barrows, 2009; Pett-Ridge, Derry, & Kurtz, 2009). Clergue et al. (2015) and Dessert et al. (2020) emphasized the important role of African dust in fertilizing a tropical rain forest in Guadeloupe and the impact of atmospheric deposition on stream water. Investigations on Quaternary age geological limestone records found on the Western Atlantic Islands of Barbados, the Florida Keys, and the Bahamas have demonstrated that Saharan dust input to these regions has existed for 875,000 years (e.g., Muhs et al., 1990, 2007). Today, satellite observations show that dust emitted from North Africa is transported to the Atlantic Ocean, and that around 50 Tg of dust reaches the Caribbean region each year (Kaufman et al., 2005). This is consistent with more refined estimates which have been made using Cloud-Aerosol Lidar with Orthogonal Polarization (CALIOP) measurements based on records spanning

Writing – original draft: Rémi Losno
Writing – review & editing: Céline Dessert, Rémi Losno

7 years (2007–2013) provided by Yu, Chin, Bian, et al. (2015). Over the past several decades, the seasonal and inter-annual variations of this transport in the Caribbean region have been observed and characterized (e.g., Prospero, 1996; Prospero et al., 1970, 2014, 2021; Prospero & Mayol-Bracero, 2013).

Particles transported to the Caribbean region from Saharan plumes are mainly composed of silicon, aluminum, and iron and have a major elemental composition close to the mean composition of the Earth's surface rocks (Goudie & Middleton, 2001; Lawrence & Neff, 2009). Marine aerosols may be the other important source of nutrients on tropical islands (e.g., Chadwick et al., 1999; Dessert et al., 2015; Eady, 1996) particularly for potassium, calcium, and magnesium, which are needed for the development of vegetation. The largest rate of deposition normally occurs in coastal regions and decreases inland as the rain scavenges sea salt (e.g., Murphy & Stallard, 2012). The emission of marine aerosols is caused by the bursting of air bubbles and clipping by the wind, both of which depend on the wind speed over the surface of the ocean (Lewis & Schwartz, 2004; Massel, 2007). The environment of the tropical rain forest is characterized by intense sources of biogenic gases and aerosols (Martin et al., 2010), as is probably the case for Guadeloupe; soil micro-organisms, vegetation, insects, and marine micro-organisms are the major biogenic sources for atmospheric deposition in the tropical coastal rain forest. North Africa could also be an important source for the long-range transport of viable micro-organisms (e.g., Prospero et al., 2005). Biogenic particles and biologic tissues are enriched in potassium, zinc, sulfur, and phosphorus (Artaxo et al., 1988; Artaxo & Maenhaut, 1990; Bowen, 1966; Martin et al., 2010). African biomass burning smoke which is well-documented at the Barbados site (Kandler et al., 2018; Kristensen et al., 2016; Quinn et al., 2022; Royer et al., 2022; Savoie et al., 2002) is another source of long-range transported elements.

Atmospheric deposition, and particularly Saharan dust, in Caribbean regions is already being investigated using different approaches:

- calculations based on the aerosol concentration with the estimated dry and wet deposition rate, and then extrapolation of the calculated results to other regions where neither deposition nor aerosol concentration measurements are available (Duce et al., 1991),
- field measurements (e.g., Morera-Gómez et al., 2019; Prospero, 1999) with extrapolations to large-scale localized field study results (Duce et al., 1991; Duce & Tindale, 1991),
- satellite observations combined with a deposition model (e.g., Engelstaedter et al., 2006),
- transport modeling (e.g., Ginoux et al., 2004; Mahowald et al., 2006),
- calculations from the mass balance of strontium isotopes in the soil (Pett-Ridge, Derry, & Barrows, 2009).

Most atmospheric deposition studies in the Caribbean have involved short-term direct deposition measurements, or indirect estimations from aerosol measurements or satellite observations for Saharan dust. Mahowald et al. (2005) pointed out the uncertainties of such estimations for iron fluxes due to spatial and temporal variability and the limited number of observations. These uncertainties reach a factor up to 10 for some fluxes estimated from satellite observations (e.g., Husar et al., 1997), and more than 50 for aerosol deduced fluxes (Heimburger et al., 2012).

Long-term studies of direct measurements of deposition fluxes are scarce. The longest study published today was conducted in Puerto Rico, where an analysis of total rainfall chemistry data spanning 20 years has been recorded (Heartsill-Scalley et al., 2007; McClintock et al., 2019). The elemental composition of atmospheric deposits was measured monthly in a highly polluted region of Cuba, from 2014 to 2016 (Morera-Gómez et al., 2019). The most documented study on trans-Atlantic dust deposition is a 3-year (from 1994 to 1996) terrestrial dust deposition record in Florida provided by Prospero et al. (2010), where both dry and wet deposition fluxes of dust were measured in nine different stations. Increasing the number and quality of the direct deposition measurements add more constraints to models and greatly improve their accuracy. These measurements are most useful when accumulated over long time periods to validate and to improve these estimations (Huneeus et al., 2011). All these studies show that it is necessary to acquire continuous atmospheric data in the Caribbean basin, over the long-term, to: (a) better investigate the contribution of dust in ecosystem nutrient cycling, in a tropical context, (b) investigate the seasonality and periodicity of this atmospheric input, and (c) improve the global aerosol models and the understanding of this environmental process.

It is therefore essential for model constraints to directly measure atmospheric deposition fluxes over long periods of time to better understand the past, present, and future of atmospheric evolution and its impact

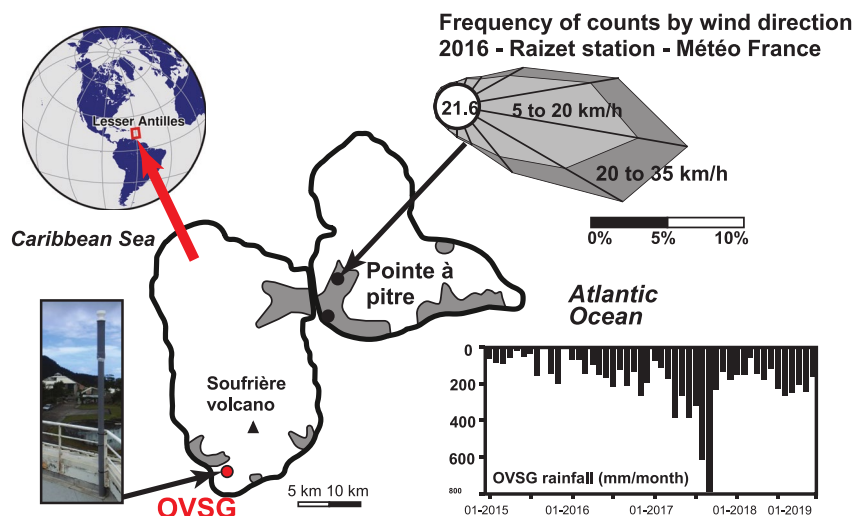


Figure 1. Sampling location and details of the sampling location on the roof of the OVSG building. $15^{\circ}58'50.84''\text{N}$, $61^{\circ}42'12.99''\text{W}$, 411 m altitude. The dominant wind direction is from left to right in the figure (from east to west). The monthly rainfall data for 2015 was measured by a rain gauge installed by Météo France at the OVSG site and the rainfall data from 2016 to the end of the sampling period is measured by a rain gauge installed by IPGP at the same place.

on the earth and the bio-geochemical system (Albani et al., 2015; Goudie & Middleton, 1992; Mahowald et al., 2010, 2011, 2014). This study presents the temporal dynamic of atmospheric deposition for major and essential elements, including Al, Fe, Na, P, Ca, Mg, K, S, and Zn, during a continuous time series from March 2015 to August 2018.

2. Materials and Methods

2.1. Site Description and Sample Collection

Basse-Terre Island is part of the Guadeloupe archipelago (Lesser Antilles, in the Caribbean Ocean), and has a surface area of 950 km². The island is characterized by a wet tropical climate, with a mean annual temperature close to 25°C and 75%–95% humidity (Chaperon et al., 1985). The Guadeloupe climate is characterized by two seasons: the dry season from approximately January to June and the cyclonic wet season from July to December. During the wet season, hurricanes and tropical depressions produce intense individual rainfall events, most of which occur in August, September, and October in Guadeloupe (Zahibo et al., 2007). The total atmospheric deposition was sampled continuously on a weekly or bimonthly basis for 41 months from March 2, 2015, to August 3, 2018, at the OVSG site (Observatoire Volcanologique et Sismologique de Guadeloupe, $15^{\circ}58'50''\text{N}$, $61^{\circ}42'13''\text{W}$, altitude: 411 m, Figure 1). The site is located at the top of Houëlmon, 9 km south-west and outside the atmospheric influence of the La Soufrière volcano, 6 km west of the nearest up-wind beach, 5 km south-west of the nearest up-wind town (Trois-Rivières). The location of the sampling site prevents any local anthropogenic contamination, especially from the urban and industrial areas of Pointe-à-Pitre (Cécé et al., 2016).

The sampling system was the same as the one described in Heimburger et al. (2012) and used hydrochloric acid instead of nitric acid as the preservative solution. Briefly, a 12 cm diameter funnel made of Teflon™ was attached to a clean 1 L polypropylene bottle pre-loaded with 50 ml of ultra-pure 3% v:v HCl aqueous solution and left open to total atmospheric deposition. The sampling system was fixed 2 m above the roof of a building and approximately 12 m above ground level (Figure 1). Each time a sample was renewed, 50 ml of a 3% v:v HCl water solution was poured into the funnel to collect the last deposits and to rinse it, and the bottle was replaced by a new one. Each sample was then weighed and completely evaporated under ultra-filtered airflow at 85°C according to the system presented in Figure S1 in Supporting Information S1. Seventeen field blanks, including an evaporation step of hundred milliliters of rinsing solution, were made to check for any possible contamination.

2.2. Analytical Method and Flux Calculation

2.2.1. Sample Digestion

All analyses were performed in clean rooms using Milli-Q™ ultra-pure water and sub-boiled ultra-pure acids. In the laboratory, 5 ml of a mixture of HCl:HF acids (3:1 v:v) was added in each evaporated bottle which was then sealed and heated on a heater plate at 70°C for at least 48 hr, producing a reflux of the acid mixture on the inner walls of the bottle. This mixture moved down the entire walls of the bottle and dissolved all of the mineral deposits. At the end of this first step, the bottle was left to cool down, its content was poured into a 60 ml Teflon™ vial and the bottle was rinsed with approximately 10 ml of water. The bottle was rinsed a second time with 3 ml of 65% HNO₃ which detached some of the remaining visible traces, likely organics, and the remainder of the contents in the bottle were recovered by rinsing the bottle twice using approximately 10 ml of water each. All of the rinsing solutions were added in the same vial as those used to collect the sample. Open vials were heated at 99°C for about 10 hr and then at 115°C until complete evaporation. During this sequence, water, hydrochloric acid, hydrofluoric acid, and silica (as SiF₄) were removed from the sample and at the end of the evaporation process, the remaining concentrated nitric acid destroyed the remaining organic matter and resulted in the full digestion of the sample. The temperature of the heater plate was then adjusted to 80°C, and 3 ml of diluted (1:1 v:v) nitric acid solution in water was added into each, now sealed, vial. After 2 hr, the full content of each vessel was completely transferred into a 125 ml polypropylene bottle (thoroughly ultra-cleaned with detergent/acid) and completed up to 100 ml with Milli-Q™ ultra-pure water. In addition, the whole Teflon vessel was also thoroughly cleaned previously, including with a blank digestion procedure.

To test the efficiency of our extraction and digestion procedures, a second extraction was performed starting from the reflux step for 13 samples (Table S1 in Supporting Information S1). The first extraction yield was calculated as the ratio between the amount extracted with the first extraction divided by the sum of the two extraction amounts. The median yield value obtained was larger than 96% for all the elements and validated a single extraction protocol.

2.2.2. Chemical Analysis

An ARCOS (Spectro-Ametek) ICP-AES equipped with a CETAC ultrasonic nebulizer or a concentric nebulizer with a cyclonic chamber was used to determine the elemental concentrations in the digested sample solutions. An external linear calibration was performed for all the analyzed elements with ICP-AES (Al, Ca, Fe, K, Mg, Na, P, S, and Zn) by measuring a set of multi-elementary solutions with a concentration between zero and 500 ppb for the calibration slope. The calibration intercept was calculated as the average of eight replicates of a blank sample (diluted ultra-pure nitric acid in Milli-Q water). Because of the well-known matrix effects in plasma with alkali metals, Na and K were also analyzed using a flame photometer (Cole Parmer 360) with an external calibration between 0 and 20 ppm. Flame photometry results were used for these two elements except for the less concentrated samples found close to or below the flame photometry detection limit, for which the ICP results were used. The wavelengths used for analysis were: 167.078 nm for Al except for the highest concentrated samples for which saturation was observed and the much less intense line at 176.641 nm was used; 317.933 nm for Ca; 238.204 nm for Fe; 285.213 nm for Mg; 177.495 nm for P; 180.731 nm for S; and 206.200 nm for Zn. For each element, the detection limit was calculated to be three times the standard deviation of the analytical blanks and converted in element masses and fluxes for each sample. The analytical relative standard deviation of the replicates was approximately 3% for values that were far above the detection limit.

Analyses of the geostandard-certified samples were performed to check the accuracy of the whole digestion and analytical methods: BE-N (SARM, Nancy, France), BHVO-1, SCO-1, MAG-1, STM-1, SDC-1 (USGS, Washington, USA). A mass between 15 and 45 mg of the previously crushed standard was placed into the same bottles which were used in the field to mimic a real deposition sample. These geostandard samples underwent the same procedures used for digestion and analysis as those for real deposition samples. The average recovery rate for each element for each geostandard is listed in Table S2 in Supporting Information S1. The recovery rates were in the range of 88%–114% (first and third quartiles) with a minimum of 70% (Ca in STM-1) and a maximum of 157% (P in BHVO-1).

2.2.3. Determination of the Saharan Dust and Sea Salt Deposition Flux

For each sample, the elemental deposition fluxes (F_i) for element i were calculated by dividing the mass of measured element i (Q_i), corrected from field blanks ($Q_{0,i}$), by the aperture area of the funnel ($S_{\text{funnel}} = 0.0113 \text{ m}^2$), and by the exposition duration (T_{exposure}). Blank data are reported in Tables S3 and S4 in Supporting Information S1.

$$F_i = \frac{Q_i - Q_{0,i}}{S_{\text{funnel}} \times T_{\text{exposure}}} \quad (1)$$

Because two samples are missing, the mean deposition flux value for a given period was calculated as the average flux measured with the existing samples:

$$F_{\text{mean}} = \frac{\sum_{\text{period}} Q_{\text{blank corrected}}}{\text{Number of sampling days} \times S_{\text{funnel}}} \quad (2)$$

The measured fluxes were broken down into three sources: North Africa dust (F_{dust}), sea salt ($F_{\text{sea salt}}$), and excess flux (F_{excess}) probably from biological sourced elements such as living materials debris (insect, plants, etc.) or microorganisms.

$$F = F_{\text{dust}} + F_{\text{seasalt}} + F_{\text{excess}} \quad (3)$$

The mass deposition fluxes of Saharan dust (F_{dust}) were estimated assuming a pure crustal origin of aluminum: $F(\text{Al}) = F(\text{Al})_{\text{dust}}$

$$F(\text{Al})_{\text{dust}} = F_{\text{Al}} = F_{\text{dust}} \text{wt}\%_{\text{Al, crust model}} F_{\text{dust}} = \frac{F_{\text{Al}}}{\text{wt}\%_{\text{Al, crust model}}} \quad (4)$$

where $\text{wt}\%_{\text{Al}}$ is the abundance of Al in the crustal soil model proposed by Rudnick and Gao (2014), equal to 8.15%.

$$F(X)_{\text{dust}} = F(\text{Al}) * (X/\text{Al})_{\text{crustal}} \quad (5)$$

Rudnick and Gao's (2014) model is used to estimate elemental ratios; $(\text{Na}/\text{Al})_{\text{crustal}} = 0.298$; $(\text{Ca}/\text{Al})_{\text{crustal}} = 0.315$; $(\text{K}/\text{Al})_{\text{crustal}} = 0.285$; $(\text{P}/\text{Al})_{\text{crustal}} = 0.00803$; $(\text{Mg}/\text{Al})_{\text{crustal}} = 0.183$; $(\text{S}/\text{Al})_{\text{crustal}} = 0.00762$; $(\text{Zn}/\text{Al})_{\text{crustal}} = 8.22 \cdot 10^{-4}$; except for iron, for which a Fe/Al ratio equal to 0.63 was proposed by Guieu et al. (2002) specifically for Saharan dust.

The mass deposition fluxes of sea salt ($F_{\text{sea salt}}$) were estimated using Brewer's (1975) model assuming that the entire Na deposition flux came from dust and sea salt (Rahn, 1976).

$$F(\text{Na}) = F(\text{Na})_{\text{dust}} + F(\text{Na})_{\text{seasalt}} \quad (6)$$

$$F(\text{Na})_{\text{seasalt}} = F(\text{Na}) - F(\text{Al}) * (\text{Na}/\text{Al})_{\text{crustal}} \quad (7)$$

$$F_{\text{seasalt}} = \frac{F(\text{Na})_{\text{seasalt}}}{\text{wt}\%_{\text{Na, seasalt model}}} \quad (8)$$

where $\text{wt}\%_{\text{Na, sea salt}}$ is equal to the sodium mass fraction in sea salt: 30.6%.

Because the concentrations of most of the major elements in sea spray were similar to those of sea salt, we used the sea salt composition (Brewer, 1975) and the $(X/\text{Na})_{\text{sea salt}}$ ratio to determine the sea salt deposition flux of the major elements $F(X)_{\text{sea salt}}$.

$$F(X)_{\text{seasalt}} = F(\text{Na})_{\text{seasalt}} (X/\text{Na})_{\text{seasalt}} \quad (9)$$

with $(\text{Ca}/\text{Na})_{\text{sea salt}} = 0.0380$; $(\text{Fe}/\text{Na})_{\text{sea salt}} = 1.8 \cdot 10^{-7}$; $(\text{K}/\text{Na})_{\text{sea salt}} = 0.0371$; $(\text{P}/\text{Na})_{\text{sea salt}} = 5.8 \cdot 10^{-6}$; $(\text{Mg}/\text{Na})_{\text{sea salt}} = 0.120$; $(\text{S}/\text{Na})_{\text{sea salt}} = 0.084$; $(\text{Zn}/\text{Na})_{\text{sea salt}} = 4.6 \cdot 10^{-7}$ (from Brewer, 1975).

The excess deposition flux after subtraction of the sea salt and dust contribution was calculated as:

$$F(X)_{\text{excess}} = F(X) - F(X)_{\text{seasalt}} - F(X)_{\text{dust}} \quad (10)$$

The enrichment factor of an element X with respect to a given source (crustal or sea salt) was calculated as:

$$EF(X)_{\text{source}} = F(X) / F(X)_{\text{source}} \quad (11)$$

3. Results and Discussion

3.1. Sampling Representativeness

Figure 1 shows the monthly rainfall (mm/month) at the OVSG site. A large inter-annual variability is observed with a dry year in 2015 contrasting with very high precipitation levels in 2017. Seasonality, with higher precipitation levels, occurs between May and November in the cyclone season of Guadeloupe, except in 2015. This seasonality is consistent with long-term observations (Jury & Bernard, 2020). The monthly rainfall ranges from 12 mm/month (May 2015) to 400 mm/month with outstanding events in August and September 2017, where rainfall reached 787 mm in 1 month due to cyclone event Maria. A median value of 151 mm/month is observed. The total rainfall values for 2015, 2016, 2017, and 2018 are 1,097, 1,796, 3,615, and 2,085 mm, respectively. Herrera and Ault (2017) highlighted the most severe drought for the Caribbean region during the 2013–2016 period, which is consistent with the lower rainfall measurement taken at OVSG in 2015 and 2016.

A good correlation is found between the collected water and rain gauge indications (Figure S2 in Supporting Information S1), up to an accumulation of 85 mm (maximum accumulation) because the rainwater overflowed the 1-L sampling bottle and therefore part of the deposition sample was lost. Corrections could not be applied to the deposited flux in this case because of unknown variations in the deposition rate during the sampling period and the subsequent heterogeneity of the sample. If accumulated, the amount of lost rainfall represents 7% of the total amount of water collected during the whole sampling period and is therefore considered negligible.

To identify potential dust sources, the periods for which the deposition flux of aluminum is higher than $2.9 \text{ mg}\cdot\text{m}^{-2}\cdot\text{day}^{-1}$ are selected because this represents the most loaded top third of the sample set. Over these periods, a backward-trajectory was calculated every hour over a period of 12 days ending 2,000 m above the sampling site using the Hysplit 4 rev. 761 model (Stein et al., 2015) based on the Global Data Assimilation System (GDAS). This backward-trajectory ensemble is plotted using the “openair” R package with the “trajLevel” function (Carslaw & Ropkins, 2012; R Core Team, 2021) showing the flyover frequencies (Figure S4 in Supporting Information S1). It can be observed that during these higher aluminum deposition flux episodes, most of the air parcels originated from the Saharan regions.

3.2. Atmospheric Deposition Fluxes of the Major Elements in Guadeloupe

The deposition fluxes averaged on the whole period ($F_{\text{whole period}}$) of each element have been reported in Table 1 and compared to the fluxes previously measured in Puerto Rico by Heartsill-Scalley et al. (2007), Cuba by Morera-Gómez et al. (2019) and Guadeloupe by Dessert et al. (2015). The larger flux was measured for Na, followed by Al, S, Mg, K, Ca, Fe, P, and Zn. Reported for the whole sampling period, the mean dust deposition flux F_{mean} is found to be $30.6 \text{ mg}\cdot\text{m}^{-2}\cdot\text{day}^{-1}$, and the mean deposition flux of sea salt is equal to $47.7 \text{ mg}\cdot\text{m}^{-2}\cdot\text{day}^{-1}$.

Figure 2 illustrates the temporal chemical flux variation for each element. The seasonality and contribution of each major source (Saharan dust, sea salt, and unknown sources are marked in different colors). It can be observed that the aluminum, iron, and calcium fluxes present a strong seasonality, with the highest deposition occurring between April and September. The potassium flux also seems to present seasonal trends but not as strong as those observed for aluminum, iron, and calcium. The trends of sodium, sulfur, and magnesium are very similar, all marked by obvious single episodes and without seasonality. The trends of the phosphorus and zinc deposition fluxes are marked by intense episodes. To understand the temporal evolution of each species, the contribution of various sources to the deposition flux of each element is investigated in the following sections.

Table 1

Mean Atmospheric Deposition Fluxes of the Major Elements in Guadeloupe (This Work) Compared to the Published Data

| | This work (2015–2018) | Cuba (2014–2016)* | Guadeloupe (2007–2008)** | Puerto-Rico (1988–2002)*** | Barbados (1999–2001)**** |
|----|--|--|--|--|--|
| | (mg.m ⁻² .day ⁻¹) |
| Al | 2.49 | 0.68 | – | – | 0.28 |
| Na | 15.3 | 2.8 | 11.2 | 24.3 | – |
| P | 0.186 | 0.103 | – | 0.300 (P-PO ₄ ³⁻) | 0.015–0.093 (dust derived) |
| K | 1.64 | 0.637 | – | 2.20 | – |
| Ca | 1.60 | 3.26 | 2.41 | 4.4 | – |
| Mg | 1.96 | 0.49 | 1.51 | 3.7 | – |
| Fe | 1.55 | 0.58 | – | – | 0.155 |
| S | 1.97 | 1.13 | 1.04 (S-SO ₄ ²⁻) | 12.6 (S-SO ₄ ²⁻) | – |
| Zn | 0.062 | 0.060 | – | – | – |

Note. *: Data from Morera-Gómez et al. (2019); **: Data from Dessert et al. (2015); ***: Data from Heartsill-Scalley et al. (2007); ****: Data from Tian et al. (2008) (for Fe and Al) and from Zamora et al. (2013) for P.

3.3. Temporal Evolution of the Saharan Dust Deposition Flux (F_{dust})

The Saharan dust deposition flux, directly derived from the aluminum deposition flux (Equation 4), presents a wide annual periodic variation, with the highest fluxes measured during the summer (from April to September). During the 41-month sampling period, the deposition flux of Saharan dust averaged over a sample period varies between 0.64 mg.m⁻².day⁻¹ (21/11/2016 to 28/11/2016) and 157 mg.m⁻².day⁻¹ (22/06/2015 to 29/06/2015). The relative amount of dust deposited during half a year between April and September represents approximately 86% for the year 2016 and 82% for the year 2017. The seasonal variation of the dust deposition was already observed in previous studies conducted in the Caribbean region, such as the Gulf of Mexico and Miami (e.g., McClintock et al., 2019; Morera-Gómez et al., 2019; Prospero & Carlson, 1981; Prospero et al., 2014).

It was possible to investigate the inter-annual variability between 1-year periods, starting at the beginning of the sampling campaign, on March 2, 2015. The dust deposition is equal to 11.0 g.m⁻² during the first year (March 2015 to February 2016), 10.2 g.m⁻² during the second year (March 2016 to February 2017), and 10.4 g.m⁻² during the third year (March 2017 to February 2018). These results show variations less than 10% for these three investigated years.

In Figure 3, we report the dust deposition fluxes for each month during the whole sampling period and the associated standard deviations deduced from the inter-annual variations. These average values take into account the monthly inter-annual variability in the intensity of the dust deposition fluxes at the 4-year scale (March 2015 to August 2018). The average dust flux is minimal in December (5.0 ± 2.0 mg.m⁻².day⁻¹) and maximal in June (75 ± 6 mg.m⁻².day⁻¹). This seasonal dust profile is consistent with the results of Prospero et al. (2014) and Prospero and Mayol-Bracero (2013), who found a similar pattern for the PM₁₀ and mineral dust atmospheric concentrations in Barbados. We note that the Saharan dust deposition flux has large standard deviations in May and October (44 ± 33 and 22 ± 16 mg.m⁻².day⁻¹, respectively), showing a large inter-annual variability of the dust deposition for these 2 months. However, this variability does not have any impact on the inter-annual variability of a full-year deposit because it only shows a shift at the beginning and end of the dust season.

Direct monthly chemical measurements in Cuba between 2014 and November 2016 (Morera-Gómez et al., 2019) are compared to the results of this work. The mean deposition flux in Cuba is equal to 8.3 mg.m⁻².day⁻¹. This flux measured in Cuba is four times lower than those measured in this work. In addition, less seasonality of dust deposition is observed in Cuba. This shows that Saharan dust transport has less of an impact at the Cuba sampling site than in Guadeloupe. This regional variation may be explained by the fact that the island of Guadeloupe is much closer to the center of the trans-Atlantic Saharan dust plume than Cuba, as demonstrated by model studies (e.g., Mahowald et al., 2006) and satellite pictures (e.g., van der Does et al., 2018). Mahowald et al. (2006) modeled an annual dust deposition flux ranging from 13.7 to 27.4 mg.m⁻².day⁻¹ in Guadeloupe and from 2.7 to 5.5 mg.m⁻².day⁻¹ in Cuba. The results obtained in this work in Guadeloupe and Morera-Gomez's (2019) results

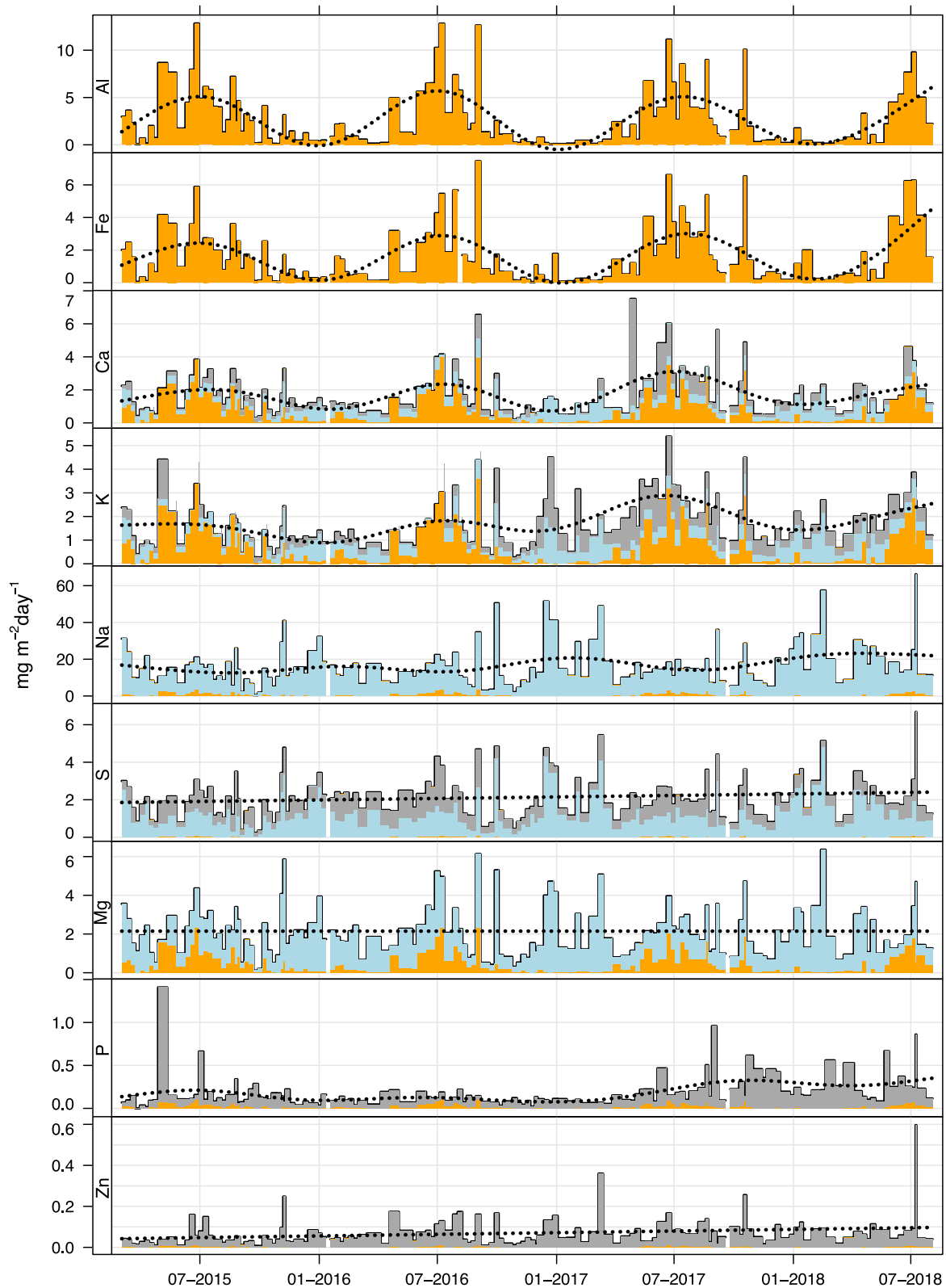


Figure 2. Deposition flux of the major elements. The source data are given in Table S5 in Supporting Information S1. The contributions of Saharan dust, sea salt, and a non-attributed source are shown in orange, light-blue, and gray. The figure is plotted using the “openair” R package with the “timePlot” function (Carslaw & Ropkins, 2012; R Core Team, 2021).

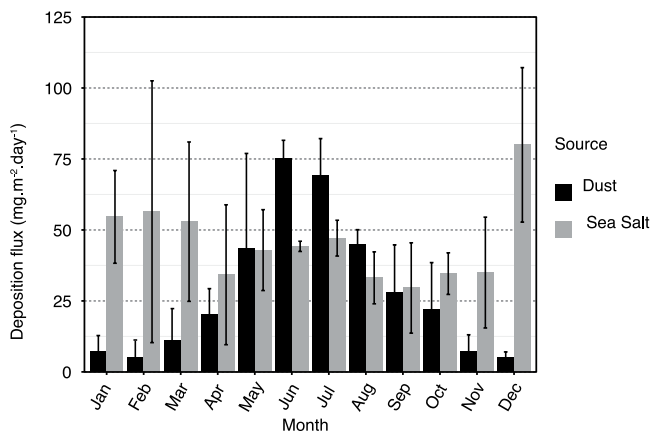


Figure 3. Monthly average deposition flux of dust and sea salt for each month and inter-annual standard deviation.

in Cuba are slightly higher than the highest model estimations but with the same relative proportion as the modeled values.

Other measurements taken in the Caribbean region are in agreement with this global spatial variability: a highest deposition flux of Saharan dust over the central part of the Caribbean basin and a lowest flux in the peripheral zone. Prospero et al. (2010) took direct measurements several decades ago with a F_{dust} value of $5.5 \text{ mg.m}^{-2}.\text{day}^{-1}$ at nine different stations in Florida, which is comparable to those measured in Cuba. Other measurements have been investigated in Puerto Rico since 1988. Heartsill-Scalley et al. (2007) estimated a mean dust deposition flux equal to $14.5 \text{ mg.m}^{-2}.\text{day}^{-1}$. McClintock et al. (2019) determined the dust deposition fluxes from the suspended solid load into open-fall rainwater samples at two different Puerto Rico stations. The deposition fluxes varied from 9.3 to $21.1 \text{ mg.m}^{-2}.\text{day}^{-1}$ during the 1988–2009 period, in agreement with the previous estimation provided by Heartsill-Scalley et al. (2007) and the modeled prediction given by Mahowald et al. (2006) of 13 – $27 \text{ mg.m}^{-2}.\text{day}^{-1}$. These values are also consistent with the geographic position of the island, that is, between Cuba and Guadeloupe.

Our results highlight that the Saharan dust deposition fluxes on the island of Guadeloupe are higher than those measured in the Northern Caribbean region, and they show that Guadeloupe is in the central part of the trans-Atlantic Saharan dust plume. This observation also matches expectations based on concentrations compared between Guadeloupe and Barbados (Prospero et al., 2014). This experimentally confirms the substantial regional variation of dust deposition between the Southeast and Northwest Caribbean, already documented by satellite observations and model studies.

3.4. Evolution of the Sea Salt Deposition Flux ($F_{\text{sea salt}}$)

Marine sea salt deposition fluxes have the same order of magnitude as dust deposition fluxes. The annual sea salt deposition fluxes in whole years beginning in March 2015 are 14.1 g.m^{-2} for the first year, 17.6 g.m^{-2} for the second year, and 18.3 g.m^{-2} for the third year. The deposition flux of sea salt averaged over each sample period varies between $1.4 \text{ mg.m}^{-2}.\text{day}^{-1}$ (September 21–28, 2015) and $213 \text{ mg.m}^{-2}.\text{day}^{-1}$ (July 8–9, 2018, during the Berly storm event). Unfortunately, no samples could be recovered during the Maria storm episode (in September 2017). The sea salt deposition flux has no obvious seasonality at our site and presents a high interannual variability for each month (Figure 3).

The model studies of Wong et al. (2020) predict that the total deposition flux of sea salt in Guadeloupe and Puerto Rico ranges between 19 and $47 \text{ mg.m}^{-2}.\text{day}^{-1}$. The highest value range is roughly consistent with our measurements for 2016 and 2017 ($46 \text{ mg.m}^{-2}.\text{day}^{-1}$) but lower than the deposition flux of $79 \text{ mg.m}^{-2}.\text{day}^{-1}$ measured in Puerto Rico by Heartsill-Scalley et al. (2007). Vet et al.'s (2014) model predicted that the total deposition flux of sea salt ranges between 6 and $10 \text{ kg.ha}^{-1}.\text{year}^{-1}$ (16 and $27 \text{ mg.m}^{-2}.\text{day}^{-1}$) for Guadeloupe and Puerto Rico, which is also lower than our direct measurements and still much lower than data from Puerto Rico. These two models did not take into account the coastal surge in Guadeloupe and Puerto Rico even though coastal surf-zones are important sources of sea salt aerosol emissions which can produce as much as 30%–50% of the total sea salt aerosol in the air of coastal regions and islands (e.g., Im, 2013). This may explain the fact that both our direct measurements and those obtained in Puerto Rico are higher than the model predictions.

It has been shown that the surface wind speed is the major driver for the sea salt aerosol emission, as a higher wind speed results in higher emission fluxes for all particle sizes of sea salt (Lewis & Schwartz, 2004; Marks, 1990; Monahan et al., 1983). Figure 4 shows the sea salt deposition fluxes as a function of wind speed assimilated near the island of Guadeloupe using 6-hourly wind data at 10 m above the up-wind sea surface (ERA-Interim; Dee et al., 2011). The data are assimilated 100 km upwind from Guadeloupe so as to take the possible coastal surge of the sea and the wind condition over the Atlantic Ocean into consideration. It can be observed that the wind speed over the Atlantic Ocean upwind of Guadeloupe also has an impact on the sea salt deposition fluxes in Guadeloupe (Figure 4). In our case, the highest deposition fluxes of sea salt often correspond to a high wind speed or heavy rain (with an average daily rainfall over 10 mm.day^{-1}) which are not necessarily cyclone events. The name of the

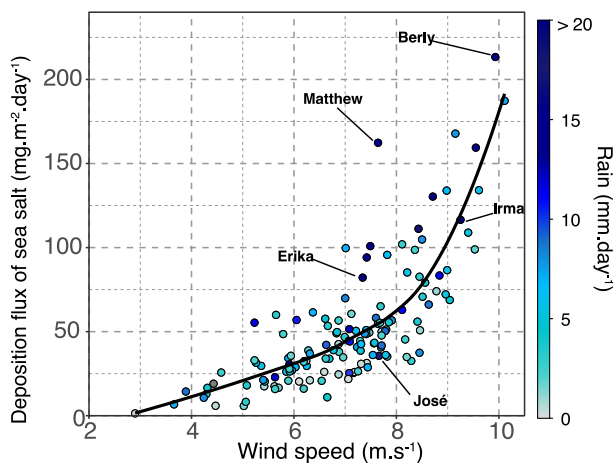


Figure 4. Sea salt deposition fluxes as a function of the averaged wind speed showing the daily precipitation rate levels (mm.day⁻¹), with the name of the five cyclone events occurring during the sampling period. The smooth correlation curve is obtained using the “ggplot2” R package with the “geom_smooth” function, to see the trend of the nonlinear relationship between two variables (R Core Team, 2021; Wickham, 2016). As the average daily rainfall ranges from 0 to 67 mm.day⁻¹ during the whole sampling period, and because only two samples correspond to a sampling period with average daily rainfall over 20 mm.day⁻¹, all the samples corresponding to daily rainfall levels over 20 mm.day⁻¹ are shown in a dark blue color.

five cyclone events occurring during the sampling period (except for Maria) have been reported in Figure 4. To investigate the influence of rainfall and wind speed on the deposition flux of sea salt, we used two Spearman correlations between the sea salt deposition fluxes and rainfall intensity, respectively (Figure S3 in Supporting Information S1). Wind speed explains 59% of the sea salt deposition flux variance whereas rainfall explains 16% of the variance, showing that wind speed is the more influential parameter controlling sea salt deposition.

To conclude, in the Caribbean region, wind as well as coastal surges may have a large impact on sea salt emission and deposition processes. Rainfall and wind patterns vary substantially over different locations, which leads to huge variations in the sea salt deposition flux, on different islands.

3.5. Contribution of Saharan Dust and Sea Salt to the Deposition Fluxes of Major Elements

3.5.1. Sources Proportion

Table 2 summarizes the respective contributions of sea salt and Saharan dust to the total deposition flux of each element during the whole sampling period, using Equations 5, 9, and 10. Sodium and magnesium are 95% and 89% explained, respectively, by the sea salt source and therefore could be considered as elements that have been sourced from sea salt alone. Fries et al. (2019), using magnesium isotopic measurements on rainwater collected in Guadeloupe, have already suggested that sea salt contributes to almost 100% of the atmospheric magnesium deposition flux. The aluminum and iron fluxes are explained with Saharan dust inputs alone. The calcium and potassium fluxes are supplied by both Saharan dust and sea salt sources, with a residue of 16% for calcium and 24% for potassium. Most of the sulfur flux is attributed to sea salt input (62%), as the crust-dust influence is negligible (1% only). For one third of the sulfur fluxes and all of the phosphorus and zinc fluxes, the source of this flux is neither sea salt nor Saharan dust. Another source must be investigated for these three elements.

3.5.2. Contribution of Biogenic and Anthropogenic Sources

Small plant debris measuring close to 100 μm have been observed under a lens in our samples, highlighting the significant biogenic input. Overall, pachosomes (~1 μm), fungal spores (~1–5 μm), plant debris (~100 μm), pollen (~5 μm), fern spores (~20 μm), and fungal hyphae (~50 μm) are present in the atmosphere and have been observed in primary biological particles collected in the Amazon Basin. They may be a local major source of aerosols in tropical forests (e.g., China et al., 2018; Martin et al., 2010). These particles may be the sources of the phosphorus, zinc, potassium, and sulfur in the samples studied here, as these elements are normally enriched in biologic tissues (e.g., Adachi et al., 2020; Barkley et al., 2021; Bowen, 1966; Fraund et al., 2017).

The presence of African biomass burning smoke in the Marine Boundary Layer is also well documented on the island of Barbados in the Caribbean region (Kristensen et al., 2016; Quinn et al., 2022; Royer et al., 2022;

Table 2
Contribution of Sea Salt and Saharan Dust to the Deposition Fluxes of the Major Elements in % (Rudnick & Gao's 2014 Model)

| Element | Al | Na | K | Ca | Mg | S | P | Fe | Zn |
|------------------------|------|-----|-----|-----|-----|-----|-------|------|-------|
| Sea salt (model)/total | 0% | 95% | 33% | 35% | 89% | 62% | 0.05% | 0% | 0.01% |
| Crust (model)/total | 100% | 5% | 43% | 49% | 23% | 1% | 11% | 101% | 3.3% |
| Excess/total | – | – | 24% | 16% | – | 37% | 89% | – | 97% |

Note. The proportion of the deposition flux derived from sea salt is calculated using Equation 9; the proportion derived from the crust is calculated using Equation 5; and the proportion of the residues is calculated using Equation 10.

Table 3
Excess Deposition Flux of Elements With a Possible Biogenic Source

| Element | K | S | P | Zn |
|--|-------|-------|------|-------|
| $F(X)_{\text{excess}}$ mg.m ⁻² .day ⁻¹ | 0.374 | 0.702 | 0.16 | 0.058 |

Note. $F(X)_{\text{excess}}$ is calculated using Equation 10.

Savoie et al., 2002). Potassium is enriched in biomass burning smoke and can be used as indicator of smoke together with black carbon (BC) and carbon monoxide (Andreae, 1983; Artaxo et al., 1994; Hand et al., 2010; Hudson et al., 2004; Li et al., 2003; Murphy et al., 2006; Pósfai et al., 2003; Reid et al., 2005). Also, African biomass burning smoke particles have been shown to contributing to sulfur deposition in South America (Ansmann et al., 2009; Barkley et al., 2019). To investigate the potential contribution of biomass burning smoke to the deposition flux of major elements in Guadeloupe island, the time series of $F(S)_{\text{excess}}$, $F(K)_{\text{excess}}$, $F(Ca)_{\text{excess}}$, $F(Zn)_{\text{excess}}$, $F(P)_{\text{excess}}$, and $F(BC)$ are plotted on Figure S5 in Supporting Information S1 together with the monthly data on atmospheric concentration of carbon monoxide, BC and the concentration of SO₂. The carbon monoxide concentration presents a marked seasonality with higher values detected between March and May. The BC concentration presents high values in August and October of each year. None of these seasonalities are clearly observed on any excess proportion of a major element of this study. We conclude that biomass burning smoke is not the major source of the excess of these elements.

The estimated mean value of the total deposition flux of BC from smoke $F(BC)_{\text{smoke}}$ is 0.134 mg.m⁻².day⁻¹ (with a min. value of 26 and a max. value of 0.67 mg.m⁻².day⁻¹, also plotted in Figure S5 in Supporting Information S1). Using the tropical forest fire smoke composition data measured by Yamasoe et al. (2000) and the African Savana biomass burning composition summarized by Reid et al. (2005), we were able to estimate the elemental ratio in the smoke. This leads to elemental ratios ranging from 0.06 to 0.3 for $(S/BC)_{\text{smoke}}$, ranging from 0.11 to 0.80 for $(K/BC)_{\text{smoke}}$, and equal to 0.008 for $(P/BC)_{\text{smoke}}$ and 0.001 for $(Zn/BC)_{\text{smoke}}$. We then roughly estimated the deposition flux derived from biomass burning smoke for these elements using the elemental ratio and deposition flux of BC: 0.008–0.041 mg.m⁻².day⁻¹ for $F(S)_{\text{smoke}}$, 0.014–0.109 mg.m⁻².day⁻¹ for $F(K)_{\text{smoke}}$, 0.001 mg.m⁻².day⁻¹ for $F(P)_{\text{smoke}}$ and 0.0001 mg.m⁻².day⁻¹ for $F(Zn)_{\text{smoke}}$. For S, P and Zn, these values are much smaller than those measured in this work (Table 3) and therefore this source could be neglected for these elements.

3.5.2.1. Potassium

On our sampling site, the excess potassium flux is 0.374 mg.m⁻².day⁻¹ accounting for one third of the total potassium deposition flux. The highest estimation of potassium coming from African biomass burning is 0.109 mg.m⁻².day⁻¹ which represents one third of the excess potassium or one tenth of the total potassium atmospheric deposition flux. Taking the uncertainties attached to these estimations into account, it is difficult to come to more quantitative conclusions on the contribution of African biomass burning.

3.5.2.2. Sulfur

The source of excess sulfur on the island of Guadeloupe can be traced to dimethyl sulfide (DMS), H₂S, or CS₂ emitted from marine or local biogenic sources (e.g., plants, microorganisms, and marine plankton) and long-range transported sources (e.g., biomass burning and anthropogenic emissions from Africa and America) (Martin et al., 2010; Vet et al., 2014). In previous studies conducted in the Caribbean region between 1988 and 1990, around 50% of nss-sulfate in aerosols has been estimated to be brought by anthropogenic emissions transported from Europe, North America, and Africa to Barbados (Savoie et al., 2002). However, it has been observed that due to the North American and European SO₂-S emission reductions in response to emission reduction programs, the wet deposition of nss-S between 2005 and 2007 is only around 50%–70% of the wet deposition of nss-S between 2000 and 2002 in the Caribbean region (Vet et al., 2014). Since then, the anthropogenic sulfur emissions in Africa have been increasing and the impact of anthropogenic sulfur on the Caribbean region is not clear. Biogenic gases containing sulfur as DMS and H₂S and the product of oxidation of these gases in the form of sulfate also exist in the marine boundary layer (Charlson et al., 1987; Huang et al., 2018; Shon et al., 2005). The excess sulfur (37%) in Guadeloupe represents a deposition flux $F(S)_{\text{excess}}$ of 0.702 mg.m⁻².day⁻¹. The Great Atlantic Sargassum belt form every year and produces massive influxes of Sargassum in the Caribbean region with substantial progression since 2015 (Wang et al., 2019). The decomposition of sargassum produces huge amounts of hydrogen sulfide (H₂S) in the atmosphere of the Caribbean coastal region which causes heavy pollution at the local scale (Cabanillas-Terán et al., 2019; Chávez et al., 2020; Rodríguez-Martínez et al., 2019). The deposition fluxes of sulfur derived from these biogenic sources are still not clearly quantified. Global model predictions neglect the impacts of sargassum decomposition at the regional scale and only take into

account the DMS produced by phytoplankton activities and, to a lesser extent, the dissolution of global anthropogenic sulfur dioxide (SO₂, e.g., Vet et al., 2014). The model predictions of Vet et al. (2014) give a range of 0.137–0.274 mg.m⁻².day⁻¹ for the wet deposition of nss-S and 0.027–0.137 mg.m⁻².day⁻¹ for the dry deposition of nss-S, leading to a total of 0.164–0.411 mg.m⁻².day⁻¹ for the deposition of nss-S. The highest value predicted by this model represents 60% of our excess sulfur measurement (0.702 mg.m⁻².day⁻¹ of excess S calculated with Equation 10), resulting in the correct order of magnitude to explain the observed amount of excess sulfur coming from large-scale DMS marine emissions. The remaining 40% of excess sulfur observed may be attributed to uncertainties and variability related to the evaluation of the DMS emission fluxes or to the still unknown contribution of the Great Atlantic Sargassum belt.

3.5.2.3. Phosphorus

Little is known about the phosphorus deposition flux all around the world because of the relatively small amount of observational data on atmospheric phosphorus and uncertainties with regard to atmospheric phosphorus sources and deposition rates (Mahowald et al., 2008; Vet et al., 2014). Phosphorus is not routinely measured during aerosol monitoring programs, these measurements are normally rare and very few long-term measurements are available (Mahowald et al., 2008; Vet et al., 2014). Model studies have concluded that the most important external source of phosphorus for tropical forests is long-range transported dust (82%), followed by long-range transported biogenic particles (12%) and biomass burning smoke (5%) (e.g., Mahowald et al., 2008; Yu, Chin, Yuan, et al., 2015).

The simulation of the atmospheric transport of phosphorus associated with mineral dust, combustion products, primary biogenic particles, marine (sea salt) aerosols, and volcanic emissions suggests a total deposition of 0.014–0.027 mg.m⁻².day⁻¹ in the North Caribbean regions. Among all the external sources of phosphorus for the Caribbean region, Saharan dust is considered as the largest source and contributes more than 90% of the total external phosphorus input (Mahowald et al., 2008). Field measurements without the influence of local emission conducted in Barbados and Miami also show that the Saharan dust is the predominant source of total phosphorus in aerosols and that contributions from sea spray, pollution, and biomass burning are minor (Zamora et al., 2013).

The deposition flux of dust-derived phosphorus roughly estimated using Zamora et al.'s (2013) measurement taken in Barbados is 0.015–0.093 mg.m⁻².day⁻¹, which supports Mahowald et al.'s (2008) model. The measured average deposition flux of phosphorus in Guadeloupe during this study $F_{\text{whole period}}$ is 0.186 mg.m⁻².day⁻¹ and the deposition flux derived from Saharan dust is 0.02 mg.m⁻².day⁻¹ (calculated from Equation 5). The phosphorus deposition flux derived from Saharan dust is within the same range as the model prediction largely based on dust from Mahowald et al. (2008) and is consistent with the rough estimation made using Zamora et al.'s (2013) measurement. The deposition flux of phosphorus roughly estimated from the BC concentration $F(\text{P})_{\text{smoke}}$ is negligible (0.001 mg.m⁻².day⁻¹). The Saharan dust-derived phosphorus $F(\text{P})_{\text{dust}}$ represents only 10.8% (9.2%–12.4%) of the measured flux. This amounts to 0.160 mg.m⁻².day⁻¹ of excess phosphorus (calculated using Equation 10) from probably local biogenic and long-range transported biogenic sources.

Almost all biogenic particles are normally highly enriched in potassium and phosphorus (Bowen, 1966). Pollen and other biogenic sources may dominate atmospheric phosphorus in and near forests or other densely vegetated areas, for example, where our sampling site is located. The importance of biogenic aerosols can be characterized as local and regional but not global (Doskey & Ugoagwu, 1989). Particles originating from plants contain substantial phosphorus levels and are considered to be the main contributor of the observed phosphorus deposition in tropical regions (Graham et al., 2003). As far as we are aware, only one publication has taken such pollen deposition and phosphorus flux measurements, around 0.083 mg.m⁻².day⁻¹ from pine pollen at a site in northern Wisconsin (Doskey & Ugoagwu, 1989), which is within the same order of magnitude as our excess phosphorus deposition flux (0.160 mg.m⁻².day⁻¹). Other recent studies conducted in the Amazon and Tropical Atlantic Ocean region with very low Saharan dust input suggest that the sources of phosphorus are more complex with substantial contributions from long-range transported African biomass burning in these regions where the Saharan dust input is minor (Ansmann et al., 2009; Barkley et al., 2019; Giglio et al., 2013; Kristensen et al., 2016; Quinn et al., 2022). However, the contribution of biomass burning smoke is estimated to be minor in regions close to Guadeloupe island in the Caribbean region (e.g., Mahowald et al., 2008; Zamora et al., 2013).

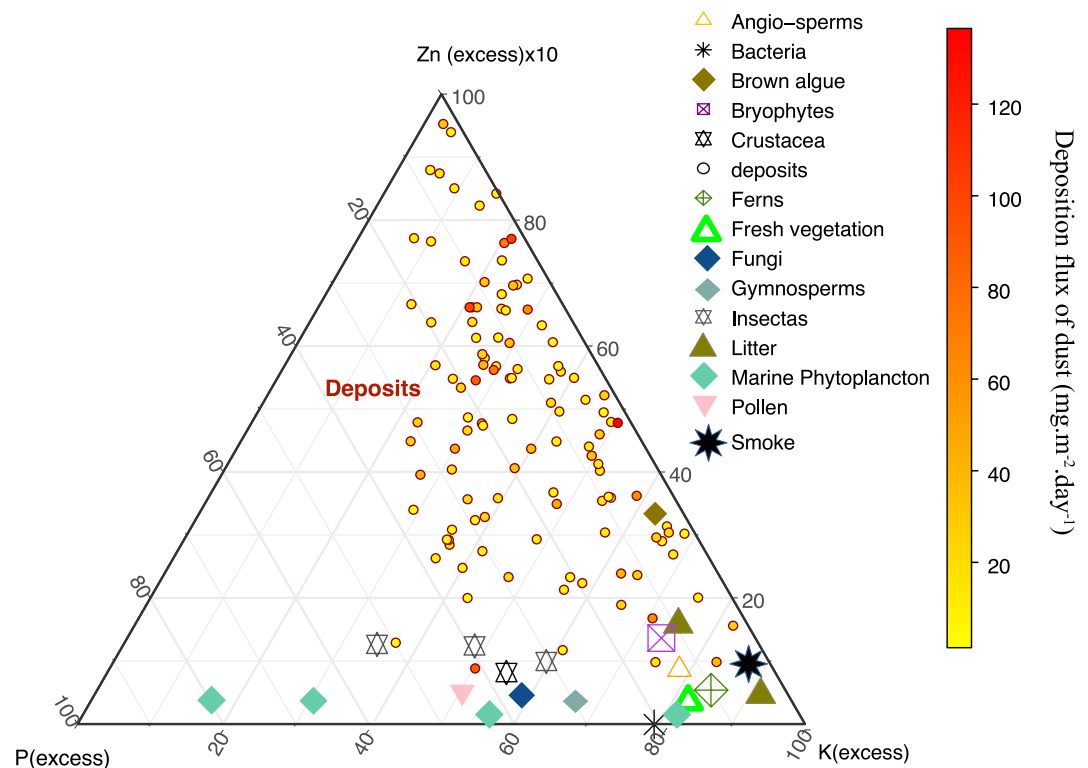


Figure 5. Ternary plot, the composition of various marine phytoplankton species are taken from Ho et al. (2003); the insect, crustacean, bacteria, fungi, bryophyte, brown algae, and angiosperm compositions are taken from Bowen (1966), the litter composition is taken from Dessert et al. (2020), the pollen composition is taken from Basso et al. (2019), the composition of the different insects' species are taken from Köhler et al. (2019), the composition of biomass burning smoke is taken from Yamasoe et al. (2000) and the fresh vegetation composition is taken from Rocha et al. (2018). The Figure is made using R with “ggtern” package (Hamilton & Ferry, 2018; R Core Team, 2021).

3.5.2.4. Zinc

With regards to both sea salt and crustal sources, 97% of the zinc is found in excess amounts. Among all samples, the crustal enrichment factor of zinc varies between 5 and 2,400 with an average value of 30; the marine enrichment factor of zinc varies between 1,200 and 70,400 with an average value of 9200. In aerosol collected near non-polluted coastal regions, a high enrichment factor of zinc up to 250,000 relative to the sea salt composition has been observed all over the world (Richardson et al., 2001). Large trace metal enrichments in the marine surface micro-layers have been reported by Duce et al. (1972). A systematic enrichment in zinc has been attributed to the marine micro-organisms and materials associated with these marine micro-organisms. It is well known that diatoms and other phytoplankton, bacteria, viruses, exopolymers, and colloidal gels are present and enriched in the sea surface micro-layer, where sea water is aerosolized (e.g., Aller et al., 2005; Bigg & Leck, 2008; Blanchard, 1975; Blanchard Duncan & Lawrence, 1970; Kuznetsova et al., 2005; Wurl & Holmes, 2008). The presence of these materials in sea spray is also well documented (e.g., Aller et al., 2017; Alpert et al., 2011; Knopf et al., 2011; Ladino et al., 2016; Wilson et al., 2015). Enrichment factors equal to 26 for phytoplankton (Sutcliffe et al., 1963) and 10–1,000 for marine bacteria (Blanchard Duncan & Lawrence, 1970) compared to the bulk seawater have been found in the literature. During phytoplankton blooms, bubble bursting generated by phytoplankton activities can produce sub-micrometer particles in the air, thereby increasing these phenomena (Hallquist et al., 2009; Kanakidou et al., 2005; Meskhidze & Nenes, 2006). However, the observed zinc enrichment factors are much higher than those found in micro-organisms and a systematic enrichment of deposit samples in zinc relative to living organisms can be observed in Figure 5. Another enrichment mechanism should therefore be investigated. Zinc in sea water may be associated with very small organically- bound aggregates of colloidal detritus present in the micro-layer. They then form relatively stable attachments at the air-sea interface by means of inter-facial forces concentrating at levels that are substantially higher than their typical crustal and sea salt abundance (Hardy, 1982). This could explain the very high enrichment factors observed.

4. Conclusion

Very different sampling techniques for atmospheric deposits are applied with variable approaches during previous studies carried out in the Caribbean region. Each of these studies examined somewhat different time periods and different sets of elements, producing large uncertainties. Before this work, long-term direct measurements of the dust deposition flux were rare. Therefore, it has been difficult to produce a consistent view of the natural atmospheric deposition flux in the Caribbean region based on current field measurement data. This study is the first continuous long-term time series (from March 2015 to August 2018) with direct measurements of elemental atmospheric deposition fluxes on the island of Guadeloupe with a resolution of days and weeks without anthropogenic influence.

The mean value of the annual deposition flux of Saharan dust was determined to be $11.2 \text{ g}\cdot\text{m}^{-2}\cdot\text{year}^{-1}$ over the 4-year sampling experiment. This value is slightly higher than recent model predictions, but within the correct order of magnitude. No inter-annual deposition flux variations were observed during this period. Saharan dust is the only source for aluminum and iron, and constitutes the largest source for calcium and potassium. A strong seasonality in the Saharan dust deposition is observed with deposition peaks between April and September, including a maximum deposition flux in July. The mean annual deposition flux value for sea salt is $17.4 \text{ g}\cdot\text{m}^{-2}\cdot\text{year}^{-1}$, with poor inter-annual variations and no seasonality. Sea salt constitutes the only source of sodium and magnesium and is a strong secondary source for calcium and potassium. The major meteorological factor influencing the sea salt deposition flux is the local wind speed.

Phosphorus deposition is strongly dominated by local biogenic sources. Biogenic particles probably originated from local insects and vegetable debris, dead or living organisms and their tissues found in sea spray. Because the measured phosphorus flux is dominated by local biogenic sources, the measured atmospheric deposition of this element cannot be related to a net atmospheric contribution but rather to an indication of local recycling. This recycling local effect must be carefully taken into account for the interpretation of phosphorus atmospheric measurements in green environments. At this stage, the phosphorus atmospheric input must be estimated from the Saharan dust input composition rather than from direct deposition measurements. Zinc is also found to have a large biogenic origin, but its enrichment factor cannot be explained by insect or vegetable debris. It should be assumed that there is a large contribution of the marine micro-layer heavily enriched with zinc.

Data Availability Statement

Data used in the creation of the manuscript are available at French Generic Research Data Center at <https://doi.org/10.57745/WEUNPS> (Losno et al., 2022) and in the Supporting Information (Table S5 in Supporting Information S1). Figures 2–4, Figures S4 and S5 in Supporting Information S1 are made with R version 4.1.1 (R Core Team, 2021) using different packages. Figure 2, Figures S4 and S5 in Supporting Information S1 are made with “openair” package version 2.9.1 (Carslaw & Ropkins, 2012). Figure 4 is made with “ggplot2” package version 3.3.5 (Wickham, 2016). Figure 5 is made with “ggtern” package version 3.3.5 (Hamilton & Ferry, 2018). Backward trajectories displayed in Figure S4 in Supporting Information S1 were calculated using the Hysplit 4 rev. 761 model (Stein et al., 2015) based on the Global Data Assimilation System (GDAS).

References

- Abouchami, W., Nätthe, K., Kumar, A., Galer, S. J. G., Jochum, K. P., Williams, E., et al. (2013). Geochemical and isotopic characterization of the Bodélé Depression dust source and implications for transatlantic dust transport to the Amazon Basin. *Earth and Planetary Science Letters*, *380*, 112–123. <https://doi.org/10.1016/j.epsl.2013.08.028>
- Adachi, K., Oshima, N., Gong, Z., de Sá, S., Bateman, A. P., Martin, S. T., et al. (2020). Mixing states of Amazon basin aerosol particles transported over long distances using transmission electron microscopy. *Atmospheric Chemistry and Physics*, *20*, 11923–11939. <https://doi.org/10.5194/acp-20-11923-2020>
- Albani, S., Mahowald, N. M., Winckler, G., Anderson, R. F., Bradtmiller, L. I., Delmonte, B., et al. (2015). Twelve thousand years of dust: The Holocene global dust cycle constrained by natural archives. *Climate of the Past*, *11*(6), 869–903. <https://doi.org/10.5194/cp-11-869-2015>
- Aller, J. Y., Kuznetsova, M. R., Jahns, C. J., & Kemp, P. F. (2005). The sea surface microlayer as a source of viral and bacterial enrichment in marine aerosols. *Journal of Aerosol Science*, *36*(5–6), 801–812. <https://doi.org/10.1016/j.jaerosci.2004.10.012>
- Aller, J. Y., Radway, J. C., Kilhau, W. P., Bothe, D. W., Wilson, T. W., Vaillancourt, R. D., et al. (2017). Size-resolved characterization of the polysaccharidic and proteinaceous components of sea spray aerosol. *Atmospheric Environment*, *154*, 331–347. <https://doi.org/10.1016/j.atmosenv.2017.01.053>
- Alpert, P. A., Aller, J. Y., & Knopf, D. A. (2011). Ice nucleation from aqueous NaCl droplets with and without marine diatoms. *Atmospheric Chemistry and Physics*, *11*(12), 5539–5555. <https://doi.org/10.5194/acp-11-5539-2011>

Acknowledgments

This work would not have been achieved without logistical support from two INSU-CNRS observatories run by the IPGP: the Observatoire Volcanologique et Sismologique de Guadeloupe (OVSG) and the Observatoire de l'Eau et de l'Erosion aux Antilles (ObsEra, OZCAR Research Infrastructure). A special thank you to Vincent Robert who helped us with the sampling, and to Jessica Chane-Teng for her work done at the beginning of this project. The authors would also like to thank S. Mullin for proofreading the English content. This work benefit of EC2CO (CNRS-INSU) support with grant “SAHAFRAN.”

- Alvarado, A. (2015). Plant nutrition in tropical forestry. In L. Pancel, & M. Köhl (Eds.), *Tropical forestry handbook* (pp. 1–91). Springer Berlin Heidelberg. https://doi.org/10.1007/978-3-642-41554-8_105-2
- Andreae, M. O. (1983). Soot carbon and excess fine potassium: Long-range transport of combustion-derived aerosols. *Science*, 220(4602), 1148–1151. <https://doi.org/10.1126/science.220.4602.1148>
- Ansmann, A., Baars, H., Tesche, M., Müller, D., Althausen, D., Engelmann, R., et al. (2009). Dust and smoke transport from Africa to South America: Lidar profiling over Cape Verde and the Amazon rainforest. *Geophysical Research Letters*, 36(11), L11802. <https://doi.org/10.1029/2009GL037923>
- Artaxo, P., Gerab, F., Yamasoe, M. A., & Martins, J. V. (1994). Fine mode aerosol composition at three long-term atmospheric monitoring sites in the Amazon Basin. *Journal of Geophysical Research*, 99(D11), 22857. <https://doi.org/10.1029/94JD01023>
- Artaxo, P., & Maenhaut, W. (1990). Trace element concentrations and size distribution of biogenic aerosols from the Amazon basin during the wet season. *Nuclear Instruments and Methods in Physics Research Section B: Beam Interactions with Materials and Atoms*, 49(1–4), 366–371. [https://doi.org/10.1016/0168-583X\(90\)90277-2](https://doi.org/10.1016/0168-583X(90)90277-2)
- Artaxo, P., Storms, H., Bruynseels, F., Van Grieken, R., & Maenhaut, W. (1988). Composition and sources of aerosols from the Amazon Basin. *Journal of Geophysical Research*, 93(D2), 1605. <https://doi.org/10.1029/JD093iD02p01605>
- Barkley, A. E., Olson, N. E., Prospero, J. M., Gatineau, A., Panechou, K., Maynard, N. G., et al. (2021). Atmospheric transport of North African dust-bearing supermicron freshwater diatoms to South America: Implications for iron transport to the Equatorial North Atlantic Ocean. *Geophysical Research Letters*, 48(5), e2020GL090476. <https://doi.org/10.1029/2020GL090476>
- Barkley, A. E., Prospero, J. M., Mahowald, N., Hamilton, D. S., Pependorf, K. J., Oehlert, A. M., et al. (2019). African biomass burning is a substantial source of phosphorus deposition to the Amazon, Tropical Atlantic Ocean, and Southern Ocean. *Proceedings of the National Academy of Sciences of the United States of America*, 116(33), 16216–16221. <https://doi.org/10.1073/pnas.1906091116>
- Basso, I. M., Lorenzo, D. S., Mouteira, M. C., & Custo, G. S. (2019). Mineral analysis of pollen by total reflection X-ray fluorescence. *Applied Radiation and Isotopes*, 152, 168–171. <https://doi.org/10.1016/j.apradiso.2019.06.015>
- Bigg, E. K., & Leck, C. (2008). The composition of fragments of bubbles bursting at the ocean surface. *Journal of Geophysical Research*, 113(D11), D11209. <https://doi.org/10.1029/2007JD009078>
- Blanchard, D. C. (1975). Bubble scavenging and the water-to-air transfer of organic material in the sea. In *Applied chemistry at protein interfaces*, Advances in chemistry (pp. 360–387). American Chemical Society. <https://doi.org/10.1021/ba-1975-0145.ch018>
- Blanchard Duncan, C., & Lawrence, S. (1970). Mechanism for the water-to-air transfer and concentration of bacteria. *Science*, 170(3958), 626–628. <https://doi.org/10.1126/science.170.3958.626>
- Bowen, H. J. M. (1966). *Trace elements in biochemistry*. Academic Press.
- Brewer, G. P. (1975). Minor elements in seawater. *Chemical Oceanography*, 1, 415–496.
- Cabanillas-Terán, N., Hernández-Arana, H. A., Ruiz-Zárate, M.-Á., Vega-Zepeda, A., & Sanchez-Gonzalez, A. (2019). *Sargassum* blooms in the Caribbean alter the trophic structure of the sea urchin *Diadema antillarum*. *PeerJ*, 7, e7589. <https://doi.org/10.7717/peerj.7589>
- Carslaw, D. C., & Ropkins, K. (2012). openair—An R package for air quality data analysis. *Environmental Modelling & Software*, 27(28), 52–61. <https://doi.org/10.1016/j.envsoft.2011.09.008>
- Cécé, R., Bernard, D., Brioude, J., & Zahibo, N. (2016). Microscale anthropogenic pollution modelling in a small tropical island during weak trade winds: Lagrangian particle dispersion simulation using real nested LES meteorological fields. *Atmospheric Environment*, 139, 98–112. <https://doi.org/10.1016/j.atmosenv.2016.05.028>
- Chadwick, O. A., Derry, L. A., Vitousek, P. M., Huebert, B. J., & Hedin, L. O. (1999). Changing sources of nutrients during four million years of ecosystem development. *Nature*, 397(6719), 491–497. <https://doi.org/10.1038/17276>
- Chaperon, P., L'Hôte, Y., & Vuillaume, G. (1985). *Les ressources en eau de surface de la Guadeloupe, Monographies hydrologiques ORSTOM*. Éd. de l'ORSTOM.
- Charlson, R. J., Lovelock, J. E., Andreae, M. O., & Warren, S. G. (1987). Oceanic phytoplankton, atmospheric sulphur, cloud albedo and climate. *Nature*, 326(6114), 655–661. <https://doi.org/10.1038/326655a0>
- Chávez, V., Uribe-Martínez, A., Cuevas, E., Rodríguez-Martínez, R. E., van Tussenbroek, B. I., Francisco, V., et al. (2020). Massive influx of pelagic *Sargassum* spp. on the coasts of the Mexican Caribbean 2014–2020: Challenges and opportunities. *Water*, 12(10), 2908. <https://doi.org/10.3390/w12102908>
- China, S., Burrows, S. M., Wang, B., Harder, T. H., Weis, J., Tanarhte, M., et al. (2018). Fungal spores as a source of sodium salt particles in the Amazon basin. *Nature Communications*, 9(1), 4793. <https://doi.org/10.1038/s41467-018-07066-4>
- Clergue, C., Dellinger, M., Buss, H. L., Gaillardet, J., Benedetti, M. F., & Dessert, C. (2015). Influence of atmospheric deposits and secondary minerals on Li isotopes budget in a highly weathered catchment, Guadeloupe (Lesser Antilles). *Chemical Geology*, 414, 28–41. <https://doi.org/10.1016/j.chemgeo.2015.08.015>
- Dee, D. P., Uppala, S. M., Simmons, A. J., Berrisford, P., Poli, P., Kobayashi, S., et al. (2011). The ERA-Interim reanalysis: Configuration and performance of the data assimilation system. *Quarterly Journal of the Royal Meteorological Society*, 137(656), 553–597. <https://doi.org/10.1002/qj.828>
- Dessert, C., Clergue, C., Rousteau, A., Crispi, O., & Benedetti, M. F. (2020). Atmospheric contribution to cations cycling in highly weathered catchment, Guadeloupe (Lesser Antilles). *Chemical Geology*, 531, 119354. <https://doi.org/10.1016/j.chemgeo.2019.119354>
- Dessert, C., Lajeunesse, E., Lloret, E., Clergue, C., Crispi, O., Gorge, C., & Quidelleur, X. (2015). Controls on chemical weathering on a mountainous volcanic tropical island: Guadeloupe (French West Indies). *Geochimica et Cosmochimica Acta*, 171, 216–237. <https://doi.org/10.1016/j.gca.2015.09.009>
- Doskey, P. V., & Ugoagwu, B. J. (1989). Atmospheric deposition of macronutrients by pollen at a semi-remote site in northern Wisconsin. *Atmospheric Environment* (1967), 23(12), 2761–2766. [https://doi.org/10.1016/0004-6981\(89\)90556-8](https://doi.org/10.1016/0004-6981(89)90556-8)
- Duce, R. A., Liss, P. S., Merrill, J. T., Atlas, E. L., Buat-Menard, P., Hicks, B. B., et al. (1991). The atmospheric input of trace species to the world ocean. *Global Biogeochemical Cycles*, 5(3), 193–259. <https://doi.org/10.1029/91GB01778>
- Duce, R. A., Quinn, J. G., Olney, C. E., Piotrowicz, S. R., Ray, B. J., & Wade, T. L. (1972). Enrichment of heavy metals and organic compounds in the surface microlayer of Narragansett Bay, Rhode Island. *Science*, 176(4031), 161–163. <https://doi.org/10.1126/science.176.4031.161>
- Duce, R. A., & Tindale, N. W. (1991). Atmospheric transport of iron and its deposition in the ocean. *Limnology & Oceanography*, 36(8), 1715–1726. <https://doi.org/10.4319/lo.1991.36.8.1715>
- Eady, R. R. (1996). Structure–function relationships of alternative nitrogenases. *Chemical Reviews*, 96(7), 3013–3030. <https://doi.org/10.1021/cr950057h>
- Engelstaedter, S., Tegen, I., & Washington, R. (2006). North African dust emissions and transport. *Earth-Science Reviews*, 79(1–2), 73–100. <https://doi.org/10.1016/j.earscirev.2006.06.004>

- Fraund, M., Pham, D., Bonanno, D., Harder, T., Wang, B., Brito, J., et al. (2017). Elemental mixing state of aerosol particles collected in Central Amazonia during GoAmazon2014/15. *Atmosphere*, 8(12), 173. <https://doi.org/10.3390/atmos8090173>
- Fries, D. M., James, R. H., Dessert, C., Bouchez, J., Beaumais, A., & Pearce, C. R. (2019). The response of Li and Mg isotopes to rain events in a highly-weathered catchment. *Chemical Geology*, 519, 68–82. <https://doi.org/10.1016/j.chemgeo.2019.04.023>
- Giglio, L., Randerson, J. T., & van der Werf, G. R. (2013). Analysis of daily, monthly, and annual burned area using the fourth-generation global fire emissions database (GFED4). *Journal of Geophysical Research: Biogeosciences*, 118(1), 317–328. <https://doi.org/10.1002/jgrg.20042>
- Ginoux, P., Prospero, J., Torres, O., & Chin, M. (2004). Long-term simulation of global dust distribution with the GOCART model: Correlation with North Atlantic Oscillation. *Environmental Modelling & Software*, 19(2), 113–128. [https://doi.org/10.1016/S1364-8152\(03\)00114-2](https://doi.org/10.1016/S1364-8152(03)00114-2)
- Goudie, A. S., & Middleton, N. J. (1992). The changing frequency of dust storms through time. *Climatic Change*, 20(3), 197–225. <https://doi.org/10.1007/BF00139839>
- Goudie, A. S., & Middleton, N. J. (2001). Saharan dust storms: Nature and consequences. *Earth-Science Reviews*, 56(1–4), 179–204. [https://doi.org/10.1016/S0012-8252\(01\)00067-8](https://doi.org/10.1016/S0012-8252(01)00067-8)
- Graham, B., Guyon, P., Maenhaut, W., Taylor, P. E., Ebert, M., Matthias-Maser, S., et al. (2003). Composition and diurnal variability of the natural Amazonian aerosol. *Journal of Geophysical Research*, 108(D24), 4765. <https://doi.org/10.1029/2003JD004049>
- Guieu, C., Loÿe-Pilot, M.-D., Ridame, C., & Thomas, C. (2002). Chemical characterization of the Saharan dust end-member: Some biogeochemical implications for the western Mediterranean Sea. *Journal of Geophysical Research*, 107(D15), 4258. <https://doi.org/10.1029/2001JD000582>
- Hallquist, M., Wenger, J. C., Baltensperger, U., Rudich, Y., Simpson, D., Claeys, M., et al. (2009). The formation, properties and impact of secondary organic aerosol: Current and emerging issues. *Atmospheric Chemistry and Physics*, 8(14), 5155–5236. <https://doi.org/10.5194/acp-9-5155-2009>
- Hamilton, N. E., & Ferry, M. (2018). ggtern: Ternary diagrams using ggplot2. *Journal of Statistical Software*, 87(3), 1–17. <https://doi.org/10.18637/jss.v087.c03>
- Hand, V. L., Capes, G., Vaughan, D. J., Formenti, P., Haywood, J. M., & Coe, H. (2010). Evidence of internal mixing of African dust and biomass burning particles by individual particle analysis using electron beam techniques. *Journal of Geophysical Research*, 115(D13), D13301. <https://doi.org/10.1029/2009JD012938>
- Hardy, J. T. (1982). The sea surface microlayer: Biology, chemistry and anthropogenic enrichment. *Progress in Oceanography*, 11(4), 307–328. [https://doi.org/10.1016/0079-6611\(82\)90001-5](https://doi.org/10.1016/0079-6611(82)90001-5)
- Heartsill-Scalley, T., Scatena, F. N., Estrada, C., McDowell, W. H., & Lugo, A. E. (2007). Disturbance and long-term patterns of rainfall and throughfall nutrient fluxes in a subtropical wet forest in Puerto Rico. *Journal of Hydrology*, 333(2–4), 472–485. <https://doi.org/10.1016/j.jhydrol.2006.09.019>
- Hedin, L. O., Granat, L., Likens, G. E., Adri Buishand, T., Galloway, J. N., Butler, T. J., & Rodhe, H. (1994). Steep declines in atmospheric base cations in regions of Europe and North America. *Nature*, 367(6461), 351–354. <https://doi.org/10.1038/367351a0>
- Heimburger, A., Losno, R., Triquet, S., Dulac, F., & Mahowald, N. (2012). Direct measurements of atmospheric iron, cobalt, and aluminum-derived dust deposition at Kerguelen Islands. *Global Biogeochemical Cycles*, 26(4), GB4016. <https://doi.org/10.1029/2012GB004301>
- Herrera, D., & Ault, T. (2017). Insights from a new high-resolution drought atlas for the Caribbean spanning 1950–2016. *Journal of Climate*, 30(19), 7801–7825. <https://doi.org/10.1175/JCLI-D-16-0838.1>
- Ho, T.-Y., Quigg, A., Finkel, Z. V., Milligan, A. J., Wyman, K., Falkowski, P. G., & Morel, F. M. M. (2003). The elemental composition of some marine phytoplankton. *Journal of Phycology*, 39(6), 1145–1159. <https://doi.org/10.1111/j.0022-3646.2003.03-090.x>
- Huang, S., Wu, Z., Poulain, L., van Pinxteren, M., Merkel, M., Assmann, D., et al. (2018). Source apportionment of the organic aerosol over the Atlantic Ocean from 53°N to 53°S: Significant contributions from marine emissions and long-range transport. *Atmospheric Chemistry and Physics*, 18(24), 18043–18062. <https://doi.org/10.5194/acp-18-18043-2018>
- Hudson, P. K., Murphy, D. M., Cziczo, D. J., Thomson, D. S., de Gouw, J. A., Warneke, C., et al. (2004). Biomass-burning particle measurements: Characteristic composition and chemical processing. *Journal of Geophysical Research*, 109(D23), D23S27. <https://doi.org/10.1029/2003JD004398>
- Huneeus, N., Schulz, M., Balkanski, Y., Griesfeller, J., Prospero, J., Kinne, S., et al. (2011). Global dust model intercomparison in AeroCom phase I. *Atmospheric Chemistry and Physics*, 11(15), 7781–7816. <https://doi.org/10.5194/acp-11-7781-2011>
- Husar, R. B., Prospero, J. M., & Stowe, L. L. (1997). Characterization of tropospheric aerosols over the oceans with the NOAA advanced very high resolution radiometer optical thickness operational product. *Journal of Geophysical Research*, 102(D14), 16889–16909. <https://doi.org/10.1029/96JD04009>
- Im, U. (2013). Impact of sea-salt emissions on the model performance and aerosol chemical composition and deposition in the East Mediterranean coastal regions. *Atmospheric Environment*, 75, 329–340. <https://doi.org/10.1016/j.atmosenv.2013.04.034>
- Jury, M. R., & Bernard, D. (2020). Climate trends in the East Antilles Islands. *International Journal of Climatology*, 40(1), 36–51. <https://doi.org/10.1002/joc.6191>
- Kanakidou, M., Seinfeld, J. H., Pandis, S. N., Barnes, I., Dentener, F. J., Facchini, M. C., et al. (2005). Organic aerosol and global climate modeling: A review. *Atmospheric Chemistry and Physics*, 7(14), 1053–1123. <https://doi.org/10.5194/acp-5-1053-2005>
- Kandler, K., Schneiders, K., Ebert, M., Hartmann, M., Weinbruch, S., Prass, M., & Pöhlker, C. (2018). Composition and mixing state of atmospheric aerosols determined by electron microscopy: Method development and application to aged Saharan dust deposition in the Caribbean boundary layer. *Atmospheric Chemistry and Physics*, 18, 13429–13455. <https://doi.org/10.5194/acp-18-13429-2018>
- Kaufman, Y. J., Koren, I., Remer, L. A., Tanré, D., Ginoux, P., & Fan, S. (2005). Dust transport and deposition observed from the Terra-Moderate Resolution Imaging Spectroradiometer (MODIS) spacecraft over the Atlantic Ocean. *Journal of Geophysical Research: Atmospheres*, 110(D10), D10S12. <https://doi.org/10.1029/2003JD004436>
- Kennedy, M. J., Chadwick, O. A., Vitousek, P. M., Derry, L. A., & Hendricks, D. M. (1998). Changing sources of base cations during ecosystem development, Hawaiian Islands. *Geology*, 26(11), 1015. [https://doi.org/10.1130/0091-7613\(1998\)026<1015:CSOBCD>2.3.CO;2](https://doi.org/10.1130/0091-7613(1998)026<1015:CSOBCD>2.3.CO;2)
- Knopf, D. A., Alpert, P. A., Wang, B., & Aller, J. Y. (2011). Stimulation of ice nucleation by marine diatoms. *Nature Geoscience*, 4(2), 88–90. <https://doi.org/10.1038/ngeo1037>
- Köhler, R., Kariuki, L., Lambert, C., & Biesalski, H. K. (2019). Protein, amino acid and mineral composition of some edible insects from Thailand. *Journal of Asia-Pacific Entomology*, 22(1), 372–378. <https://doi.org/10.1016/j.aspen.2019.02.002>
- Koren, I., Kaufman, Y. J., Washington, R., Todd, M. C., Rudich, Y., Martins, J. V., & Rosenfeld, D. (2006). The Bodélé depression: A single spot in the Sahara that provides most of the mineral dust to the Amazon forest. *Environmental Research Letters*, 1, 014005. <https://doi.org/10.1088/1748-9326/1/1/014005>
- Kristensen, T. B., Müller, T., Kandler, K., Benker, N., Hartmann, M., Prospero, J. M., et al. (2016). Properties of cloud condensation nuclei (CCN) in the trade wind marine boundary layer of the western North Atlantic. *Atmospheric Chemistry and Physics*, 16(4), 2675–2688. <https://doi.org/10.5194/acp-16-2675-2016>

- Kumar, A., Abouchami, W., Galer, S. J. G., Garrison, V. H., Williams, E., & Andreae, M. O. (2014). A radiogenic isotope tracer study of transatlantic dust transport from Africa to the Caribbean. *Atmospheric Environment*, 82, 130–143. <https://doi.org/10.1016/j.atmosenv.2013.10.021>
- Kuznetsova, M., Lee, C., & Aller, J. (2005). Characterization of the proteinaceous matter in marine aerosols. *Marine Chemistry*, 96(3–4), 359–377. <https://doi.org/10.1016/j.marchem.2005.03.007>
- Ladino, L. A., Yakobi-Hancock, J. D., Kilhau, W. P., Mason, R. H., Si, M., Li, J., et al. (2016). Addressing the ice nucleating abilities of marine aerosol: A combination of deposition mode laboratory and field measurements. *Atmospheric Environment*, 132, 1–10. <https://doi.org/10.1016/j.atmosenv.2016.02.028>
- Lawrence, C. R., & Neff, J. C. (2009). The contemporary physical and chemical flux of aeolian dust: A synthesis of direct measurements of dust deposition. *Chemical Geology*, 267(1–2), 46–63. <https://doi.org/10.1016/j.chemgeo.2009.02.005>
- Lewis, E. R., & Schwartz, S. E. (2004). Sea salt aerosol production: Mechanisms, methods, measurements and models; A critical review. In *Geophysical Monograph*. American Geophysical Union.
- Li, J., Pósfai, M., Hobbs, P. V., & Buseck, P. R. (2003). Individual aerosol particles from biomass burning in southern Africa: 2. Compositions and aging of inorganic particles. *Journal of Geophysical Research*, 108(D13), 8484. <https://doi.org/10.1029/2002JD002310>
- Losno, R., Xu-Yang, Y., Dessert, C. (2022). Atmospheric deposition flux of major and biogenic elements over Guadeloupe (2015–2018) [Dataset]. Recherche Data Gouv, V1, UNF:6:GdNlnGLPpdlyArCHhbRAtA== [fileUNF]. <https://doi.org/10.57745/WEUNPS>
- Mahowald, N. M., Albani, S., Kok, J. F., Engelstaedter, S., Scanza, R., Ward, D. S., & Flanner, M. G. (2014). The size distribution of desert dust aerosols and its impact on the Earth system. *Aeolian Research*, 15, 53–71. <https://doi.org/10.1016/j.aeolia.2013.09.002>
- Mahowald, N. M., Baker, A. R., Bergametti, G., Brooks, N., Duce, R. A., Jickells, T. D., et al. (2005). Atmospheric global dust cycle and iron inputs to the ocean. *Global Biogeochemical Cycles*, 19(4), GB4025. <https://doi.org/10.1029/2004GB002402>
- Mahowald, N. M., Jickells, T. D., Baker, A. R., Artaxo, P., Benitez-Nelson, C. R., Bergametti, G., et al. (2008). Global distribution of atmospheric phosphorus sources, concentrations and deposition rates, and anthropogenic impacts. *Global Biogeochemical Cycles*, 22(4), GB4026. <https://doi.org/10.1029/2008GB003240>
- Mahowald, N. M., Kloster, S., Engelstaedter, S., Moore, J. K., Mukhopadhyay, S., McConnell, J. R., et al. (2010). Observed 20th century desert dust variability: Impact on climate and biogeochemistry. *Atmospheric Chemistry and Physics*, 10(22), 10875–10893. <https://doi.org/10.5194/acp-10-10875-2010>
- Mahowald, N. M., Muhs, D. R., Levis, S., Rasch, P. J., Yoshioka, M., Zender, C. S., & Luo, C. (2006). Change in atmospheric mineral aerosols in response to climate: Last glacial period, preindustrial, modern, and doubled carbon dioxide climates. *Journal of Geophysical Research*, 111(D10), D10202. <https://doi.org/10.1029/2005JD006653>
- Mahowald, N. M., Ward, D. S., Kloster, S., Flanner, M. G., Heald, C. L., Heavens, N. G., et al. (2011). Aerosol impacts on climate and biogeochemistry. *Annual Review of Environment and Resources*, 36(1), 45–74. <https://doi.org/10.1146/annurev-environ-042009-094507>
- Marks, R. (1990). Preliminary investigations on the influence of rain on the production, concentration, and vertical distribution of sea salt aerosol. *Journal of Geophysical Research: Oceans*, 95(C12), 22299–22304. <https://doi.org/10.1029/JC095C12p22299>
- Martin, S. T., Andreae, M. O., Artaxo, P., Baumgardner, D., Chen, Q., Goldstein, A. H., et al. (2010). Sources and properties of Amazonian aerosol particles. *Reviews of Geophysics*, 48(2), RG2002. <https://doi.org/10.1029/2008RG000280>
- Martin, J. H., & Fitzwater, S. E. (1988). Iron deficiency limits phytoplankton growth in the north-east Pacific subarctic. *Nature*, 331(6154), 341–343. <https://doi.org/10.1038/331341a0>
- Massel, S. R. (2007). *Ocean waves breaking and marine aerosol fluxes, atmospheric and oceanographic sciences library*. Springer New York. <https://doi.org/10.1007/978-0-387-69092-6>
- McClintock, M. A., Brocard, G., Willenbring, J., Tamayo, C., Porder, S., & Pett-Ridge, J. C. (2015). Spatial variability of African dust in soils in a montane tropical landscape in Puerto Rico. *Chemical Geology*, 412, 69–81. <https://doi.org/10.1016/j.chemgeo.2015.06.032>
- McClintock, M. A., McDowell, W. H., González, G., Schulz, M., & Pett-Ridge, J. C. (2019). African dust deposition in Puerto Rico: Analysis of a 20-year rainfall chemistry record and comparison with models. *Atmospheric Environment*, 216, 116907. <https://doi.org/10.1016/j.atmosenv.2019.116907>
- Meskhidze, N., & Nees, A. (2006). Phytoplankton and cloudiness in the Southern Ocean. *Science*, 314(5804), 1419–1423. <https://doi.org/10.1126/science.1131779>
- Monahan, E. C., Fairall, C. W., Davidson, K. L., & Boyle, P. J. (1983). Observed inter-relations between 10m winds, ocean whitecaps and marine aerosols. *Quarterly Journal of the Royal Meteorological Society*, 109(460), 379–392. <https://doi.org/10.1002/qj.49710946010>
- Morera-Gómez, Y., Santamaría, J. M., Elustondo, D., Lasheras, E., & Alonso-Hernández, C. M. (2019). Determination and source apportionment of major and trace elements in atmospheric bulk deposition in a Caribbean rural area. *Atmospheric Environment*, 202, 93–104. <https://doi.org/10.1016/j.atmosenv.2019.01.019>
- Muhs, D. R., Budahn, J. R., Prospero, J. M., & Carey, S. N. (2007). Geochemical evidence for African dust inputs to soils of western Atlantic islands: Barbados, the Bahamas, and Florida. *Journal of Geophysical Research*, 112(F2), F02009. <https://doi.org/10.1029/2005JF000445>
- Muhs, D. R., Bush, C. A., Stewart, K. C., Rowland, T. R., & Crittenden, R. C. (1990). Geochemical evidence of Saharan dust parent material for soils developed on Quaternary limestones of Caribbean and Western Atlantic islands. *Quaternary Research*, 33(2), 157–177. [https://doi.org/10.1016/0033-5894\(90\)90016-E](https://doi.org/10.1016/0033-5894(90)90016-E)
- Murphy, D. M., Cziczo, D. J., Froyd, K. D., Hudson, P. K., Matthew, B. M., Middlebrook, A. M., et al. (2006). Single-particle mass spectrometry of tropospheric aerosol particles. *Journal of Geophysical Research*, 111(D23), D23S32. <https://doi.org/10.1029/2006JD007340>
- Murphy, S. F., & Stallard, R. F. (Eds.) (2012). *Water quality and landscape processes of four watersheds in eastern Puerto Rico*. U.S. Geological Survey.
- Okin, G. S., Baker, A. R., Tegen, I., Mahowald, N. M., Dentener, F. J., Duce, R. A., et al. (2011). Impacts of atmospheric nutrient deposition on marine productivity: Roles of nitrogen, phosphorus, and iron. *Global Biogeochemical Cycles*, 25(2), GB2022. <https://doi.org/10.1029/2010GB003858>
- Okin, G. S., Mahowald, N., Chadwick, O. A., & Artaxo, P. (2004). Impact of desert dust on the biogeochemistry of phosphorus in terrestrial ecosystems. *Global Biogeochemical Cycles*, 18(2), GB2005. <https://doi.org/10.1029/2003GB002145>
- Pett-Ridge, J. C., Derry, L. A., & Barrows, J. K. (2009). Ca/Sr and 87Sr/86Sr ratios as tracers of Ca and Sr cycling in the Rio Icacos watershed, Luquillo Mountains, Puerto Rico. *Chemical Geology*, 267(1–2), 32–45. <https://doi.org/10.1016/j.chemgeo.2008.11.022>
- Pett-Ridge, J. C., Derry, L. A., & Kurtz, A. C. (2009). Sr isotopes as a tracer of weathering processes and dust inputs in a tropical granitoid watershed, Luquillo Mountains, Puerto Rico. *Geochimica et Cosmochimica Acta*, 73(1), 25–43. <https://doi.org/10.1016/j.gca.2008.09.032>
- Pósfai, M., Simonic, R., Li, J., Hobbs, P. V., & Buseck, P. R. (2003). Individual aerosol particles from biomass burning in southern Africa: 1. Compositions and size distributions of carbonaceous particles. *Journal of Geophysical Research*, 108(D13), 8483. <https://doi.org/10.1029/2002JD002291>

- Prospero, J. M. (1996). Saharan dust transport over the North Atlantic Ocean and Mediterranean: An Overview. In S. Guerzoni, & R. Chester (Eds.), *The impact of desert dust across the Mediterranean*. (pp. 133–151). Springer Netherlands. https://doi.org/10.1007/978-94-017-3354-0_13
- Prospero, J. M. (1999). Long-term measurements of the transport of African mineral dust to the southeastern United States: Implications for regional air quality. *Journal of Geophysical Research*, *104*(D13), 15917–15927. <https://doi.org/10.1029/1999JD900072>
- Prospero, J. M., Barkley, A. E., Gaston, C. J., Gatineau, A., Campos y Sansano, A., & Panechou, K. (2020). Characterizing and quantifying African dust transport and deposition to South America: Implications for the phosphorus budget in the Amazon Basin. *Global Biogeochemical Cycles*, *34*(9), e2020GB006536. <https://doi.org/10.1029/2020GB006536>
- Prospero, J. M., Blades, E., Mathison, G., & Naidu, R. (2005). Interhemispheric transport of viable fungi and bacteria from Africa to the Caribbean with soil dust. *Aerobiologia*, *21*, 1–19. <https://doi.org/10.1007/s10453-004-5872-7>
- Prospero, J. M., Bonatti, E., Schubert, C., & Carlson, T. N. (1970). Dust in the Caribbean atmosphere traced to an African dust storm. *Earth and Planetary Science Letters*, *9*(3), 287–293. [https://doi.org/10.1016/0012-821X\(70\)90039-7](https://doi.org/10.1016/0012-821X(70)90039-7)
- Prospero, J. M., & Carlson, T. N. (1981). Saharan air outbreaks over the tropical North Atlantic. *PAGEOPH*, *119*(3), 677–691. <https://doi.org/10.1007/BF00878167>
- Prospero, J. M., Collard, F.-X., Molinié, J., & Jeannot, A. (2014). Characterizing the annual cycle of African dust transport to the Caribbean Basin and South America and its impact on the environment and air quality: African dust transport to South America. *Global Biogeochemical Cycles*, *28*(7), 757–773. <https://doi.org/10.1002/2013GB004802>
- Prospero, J. M., Delany, A. C., Delany, A. C., & Carlson, T. N. (2021). The discovery of African dust transport to the Western Hemisphere and the Saharan air layer: A history. *Bulletin of the American Meteorological Society*, *102*(6), E1239–E1260. <https://doi.org/10.1175/BAMS-D-19-0309.1>
- Prospero, J. M., Landing, W. M., & Schulz, M. (2010). African dust deposition to Florida: Temporal and spatial variability and comparisons to models. *Journal of Geophysical Research*, *115*(D13), D13304. <https://doi.org/10.1029/2009JD012773>
- Prospero, J. M., & Mayol-Bracero, O. L. (2013). Understanding the transport and impact of African dust on the Caribbean Basin. *Bulletin of the American Meteorological Society*, *94*(9), 1329–1337. <https://doi.org/10.1175/BAMS-D-12-00142.1>
- Quinn, P. K., Bates, T. S., Coffman, D. J., Upchurch, L. M., Johnson, J. E., Brewer, A., et al. (2022). Wintertime observations of tropical North-west Atlantic aerosol properties during ATOMIC: Varying mixtures of dust and biomass burning. *Journal of Geophysical Research: Atmospheres*, *127*(8), e2021JD036253. <https://doi.org/10.1029/2021JD036253>
- Rahn, K. A. (1976). *The chemical composition of the atmospheric aerosol*. Graduate School of Oceanography, University of Rhode Island.
- R Core Team. (2021). R: A language and environment for statistical computing [Software]. R Foundation for Statistical Computing. Retrieved from <https://www.R-project.org/>
- Reid, J. S., Koppmann, R., Eck, T. F., & Eleuterio, D. P. (2005). A review of biomass burning emissions: Part II: Intensive physical properties of biomass burning particles. *Atmospheric Chemistry and Physics*, *5*(3), 799–825. <https://doi.org/10.5194/acp-5-799-2005>
- Richardson, M., Garrett, R., Mitchell, I., Mah-Paulson, M., & Hackbarth, T. (2001). *Critical review on natural global and regional emissions of six trace metals to the atmosphere* (59 pp.). International Lead Zinc Research Organization (ILRZRO). https://echa.europa.eu/documents/10162/17228/vrar_appendix_p2_en.pdf/970fdd97-abc8-40c5-92cf-029fa47c09b5
- Rocha, L. S., Gonçalves, D. A., Arakaki, D. G., Tschinkel, P. F. S., de Lima, N. V., de Oliveira, L. C. S., et al. (2018). Data on elemental composition of the medicinal plant *Hymenaea martiana* Hayne (Jatobá). *Data in Brief*, *19*, 959–964. <https://doi.org/10.1016/j.dib.2018.05.142>
- Rodríguez-Martínez, R. E., Medina-Valmaseda, A. E., Blanchon, P., Monroy-Velázquez, L. V., Almazán-Becerril, A., Delgado-Pech, B., et al. (2019). Faunal mortality associated with massive beaching and decomposition of pelagic Sargassum. *Marine Pollution Bulletin*, *146*, 201–205. <https://doi.org/10.1016/j.marpolbul.2019.06.015>
- Royer, H. M., Pöhlker, M. L., Krüger, O., Blades, E., Sealy, P., Lata, N. N., et al. (2022). African smoke particles act as cloud condensation nuclei in the wintertime tropical North Atlantic boundary layer over Barbados (preprint). In *Aerosols/Field Measurements/Troposphere/Chemistry (Chemical Composition and Reactions)*. <https://doi.org/10.5194/acp-2022-341>
- Rudnick, R. L., & Gao, S. (2014). Composition of the continental crust. In *Treatise on geochemistry* (pp. 1–51). Elsevier. <https://doi.org/10.1016/B978-0-08-095975-7.00301-6>
- Savoie, D. L., Arimoto, R., Keene, W. C., Prospero, J. M., Duce, R. A., & Galloway, J. N. (2002). Marine biogenic and anthropogenic contributions to non-sea-salt sulfate in the marine boundary layer over the North Atlantic Ocean. *Journal of Geophysical Research*, *107*(D18), 4356. <https://doi.org/10.1029/2001JD000970>
- Shon, Z.-H., Kim, K.-H., Swan, H., Lee, G., & Kim, Y.-K. (2005). DMS photochemistry during the Asian dust-storm period in the Spring of 2001: Model simulations vs. field observations. *Chemosphere*, *58*(2), 149–161. <https://doi.org/10.1016/j.chemosphere.2004.09.014>
- Stein, A. F., Draxler, R. R., Rolph, G. D., Stunder, B. J. B., Cohen, M. D., & Ngan, F. (2015). NOAA's HYSPLIT atmospheric transport and dispersion modeling system. *Bulletin of the American Meteorological Society*, *96*(12), 2059–2077. <https://doi.org/10.1175/BAMS-D-14-00110.1>
- Sutcliffe, W. H., Baylor, E. R., & Menzel, D. W. (1963). Sea surface chemistry and Langmuir circulation. *Deep Sea Research and Oceanographic Abstracts*, *10*(3), 233–243. [https://doi.org/10.1016/0011-7471\(63\)90359-0](https://doi.org/10.1016/0011-7471(63)90359-0)
- Tian, Z., Ollivier, P., Véron, A., & Church, T. M. (2008). Atmospheric Fe deposition modes at Bermuda and the adjacent Sargasso Sea. *Geochemistry, Geophysics, Geosystems*, *9*(8), Q08007. <https://doi.org/10.1029/2007GC001868>
- van der Does, M., Pourmand, A., Sharifi, A., & Stuut, J.-B. W. (2018). North African mineral dust across the tropical Atlantic Ocean: Insights from dust particle size, radiogenic Sr-Nd-Hf isotopes and rare Earth elements (REE). *Aeolian Research*, *33*, 106–116. <https://doi.org/10.1016/j.aeolia.2018.06.001>
- Vet, R., Artz, R. S., Carou, S., Shaw, M., Ro, C.-U., Aas, W., et al. (2014). A global assessment of precipitation chemistry and deposition of sulfur, nitrogen, sea salt, base cations, organic acids, acidity and pH, and phosphorus. *Atmospheric Environment*, *93*, 3–100. <https://doi.org/10.1016/j.atmosenv.2013.10.060>
- Wang, M., Hu, C., Barnes, B. B., Mitchum, G., Lapointe, B., & Montoya, J. P. (2019). The great Atlantic Sargassum belt. *Science*, *365*(6448), 83–87. <https://doi.org/10.1126/science.aaw7912>
- Wickham, H. (2016). *ggplot2*. Use R! Springer International Publishing. <https://doi.org/10.1007/978-3-319-24277-4>
- Wilson, T. W., Ladino, L. A., Alpert, P. A., Breckels, M. N., Brooks, I. M., Browne, J., et al. (2015). A marine biogenic source of atmospheric ice-nucleating particles. *Nature*, *525*(7568), 234–238. <https://doi.org/10.1038/nature14986>
- Wong, M. Y., Mahowald, N. M., Marino, R., Williams, E. R., Chellam, S., & Howarth, R. W. (2020). Natural atmospheric deposition of molybdenum: A global model and implications for tropical forests. *Biogeochemistry*, *149*(2), 159–174. <https://doi.org/10.1007/s10533-020-00671-w>
- Wurl, O., & Holmes, M. (2008). The gelatinous nature of the sea-surface microlayer. *Marine Chemistry*, *110*(1–2), 89–97. <https://doi.org/10.1016/j.marchem.2008.02.009>

- Yamasoe, M. A., Artaxo, P., Miguel, A. H., & Allen, A. G. (2000). Chemical composition of aerosol particles from direct emissions of vegetation fires in the Amazon Basin: Water-soluble species and trace elements. *Atmospheric Environment*, *34*(10), 1641–1653. [https://doi.org/10.1016/S1352-2310\(99\)00329-5](https://doi.org/10.1016/S1352-2310(99)00329-5)
- Yu, H., Chin, M., Bian, H., Yuan, T., Prospero, J. M., Omar, A. H., et al. (2015). Quantification of trans-Atlantic dust transport from seven-year (2007–2013) record of CALIPSO lidar measurements. *Remote Sensing of Environment*, *159*, 232–249. <https://doi.org/10.1016/j.rse.2014.12.010>
- Yu, H., Chin, M., Yuan, T., Bian, H., Remer, L. A., Prospero, J. M., et al. (2015). The fertilizing role of African dust in the Amazon rainforest: A first multiyear assessment based on data from cloud-aerosol lidar and infrared pathfinder satellite observations. *Geophysical Research Letters*, *42*(6), 1984–1991. <https://doi.org/10.1002/2015GL063040>
- Zahibo, N., Pelinovsky, E., Talipova, T., Rabinovich, A., Kurkin, A., & Nikolkina, I. (2007). Statistical analysis of cyclone hazard for Guadeloupe, Lesser Antilles. *Atmospheric Research*, *84*(1), 13–29. <https://doi.org/10.1016/j.atmosres.2006.03.008>
- Zamora, L. M., Prospero, J. M., Hansell, D. A., & Trapp, J. M. (2013). Atmospheric P deposition to the subtropical North Atlantic: Sources, properties, and relationship to N deposition. *Journal of Geophysical Research: Atmospheres*, *118*(3), 1546–1562. <https://doi.org/10.1002/jgrd.50187>